# A Study of Directionally Solidified Rene 80 Subjected to Short-term Overtemperature

**Heather D. M. Smart**

Thesis submitted to the Faculty of Graduate Studies of the University of Manitoba in partial fulfillment of the requirements for the degree of

**Master of Science**
in
**Mechanical and Manufacturing Engineering**
**University of Manitoba**

Winnipeg, Manitoba
**February 2017**

# Acknowledgements

This Masters program was intended to encompass only two years. It has been prolonged and resulted in a learning experience that has surprised me. In addition to academic achievement, this process has been an exercise in perseverance, patience and personal growth.

Thank you to my academic advisors, Dr. Norman Richards and Dr. Olanrewaju Ojo, to my industrial advisor, Brent Junkin, to the staff and other students in the metallurgical department and to Krutika Vishwakarma, for all of her one-on-one assistance early on in the research phase. Thank you also to the Materials & Mechatronics Lab personnel at University of Waterloo, particularly Dr. Mary Wells, for allowing my visit and Mark Whitney, for his efforts in helping me complete my research.

Thank you to Dr. Laura L. Murray, for her support, advice and contribution to my progress. And, to my family: Kelsey, Duncan and Lindsay, who have often helped without knowing it, as well as completed the odd legitimate task over the past few years. Ian, it is possible for me to have done this without you, but I feel like you are partly responsible for everything I accomplish. Thank you for being there.

# Abstract

The effects of short-term overtemperature on the properties of turbine blade superalloys have historically been conservatively estimated and limited published data on the condition are available. Gamma prime (γ′) is the main strengthening constituent of Rene 80, a directionally solidified (DS), nickel-based superalloy typical of turbine blade substrate material. Short-term overtemperature describes an engine condition during which the engine is observed to operate at a temperature beyond specifications for a time period not exceeding 60 seconds. This condition is considered a risk factor due to potential for initiating the dissolution of the γ′ constituent into the gamma (γ) matrix, resulting in reduced material strength. Discrete experiments were conducted on Rene 80, precipitation heat-treated to a condition of favourable volume fraction of γ'-γ, to observe the effects of temperature, time and tensile loading. Temperature-dependent testing showed evidence of a solvus temperature range of approximately 1130 ºC - 1190 ºC, with some dissolution occurring at 1130 ºC, and full dissolution of γ' having essentially occurred at 1190 ºC, for short-term hold time (1 second). A shift from solid-state to liquid state dissolution was observed in the temperature-dependent samples. Time-dependent testing conducted at 1150 ºC, the "practical dissolution temperature" of γ', showed increasing dissolution with increasing time. Load-dependent testing produced reduced volume fraction of γ' for samples tested with a tensile load, when compared to unloaded samples, and the effect of stress was more pronounced at test temperature of 1150 ºC versus 1050 ºC. Dissolution was not consistent throughout the stress-dependent samples. The mechanisms by which dissolution is occurring in the various samples are explained and relevant theories which support reported observations are then discussed and summarized.

# Table of Contents

# List of Figures

# List of Tables

# Chapter 1

## Introduction

Alloys of nickel, cobalt, or iron, together with elements such as aluminum, chromium, and titanium and some refractory elements such as molybdenum, tantalum and tungsten and possessing the characteristic of a precipitate strengthening phase induced by heat treatment, fall into a category of metal alloys known as superalloys. Nickel-base superalloys, developed for use primarily in gas turbine engines, experienced improvements and modifications throughout the latter part of the twentieth century in order to solve problems caused by specific operational conditions of these turbine engines such as heat cycling, load cycling and the presence of corrosive and oxide-forming gases. In the pursuit of increasing engine efficiency, superalloys are critical in allowing for higher operating temperature without increasing size or weight of an engine. In the pursuit of increasing engine life, superalloys are dependable at maintaining good mechanical strength and surface stability by retaining a high volume fraction of the strengthening precipitate phase. [1, 2] Nickel-base superalloys are consistently used in the combustion section or in immediate proximity to gas path within the turbine section as the substrate material for components such as combustion liners, first stage turbine nozzles and first stage turbine blades. At operating temperatures approaching the practical melting temperature of these alloys (approximately $0.7 - 0.8T_M$), components are required to withstand significant load cycling without experiencing significant structural deterioration. [1, 3]

In order to ensure flight safety, every aircraft engine is designed with a series of operational limits to be observed during flight. Since operating temperature is directly related to the output

power of the engine, as well as directly affects life of components, it is typically a closely-monitored specification, either as Turbine Inlet Temperature (TIT) or Inter-Turbine Temperature (ITT). Temperature limits for different conditions of operation such as starting, ground idle, normal cruise and maximum power are developed taking into account, among other things, the capabilities of materials of critical components. During operation of the engine, if any of these limits is exceeded beyond a specified length of time (beyond 1000ºC for longer than 5 seconds, for example), the condition may be designated as a "short-term over-temperature," cause for engine removal from the aircraft as well as removal and disposal of the turbine blades. Metallurgical assessment of first-stage turbine blades is included within the disposition instructions once an engine has been removed for the condition of over-temperature. This assessment typically requires cross-section of the blade for preparation as a metallurgical sample, inherently a destructive process requiring replacement of the blades, which is often a costly alternative. It is therefore prudent to understand the effects of exceeding engine specifications on the components.

In nickel superalloys, the primary strengthening factor is the constituent called gamma prime (γ'), a material phase that precipitates from the solid-solution matrix of nickel, the gamma (γ) phase when material is exposed to a specific temperature range. For blade assessment, observation of the ratio of gamma-prime phase precipitates to gamma-phase matrix and overall ratio of gamma prime to gamma (γ':γ) in the questionable blades is qualitatively compared to that of an acceptable sample. Traditionally, technicians in industry utilize optical microscopy as a primary method for this assessment. However, due to size of gamma prime in DS Rene 80 measuring approximately 0.5 μm in width when the material is in the precipitation heat-treated state, such an evaluation method may be considered beyond the resolution limit of many optical

microscopes. Scanning electron microscope (SEM) which has resolution capabilities considerably beyond optical microscope is therefore used in acquiring data for the present work.

Due to the competitive nature of the aerospace industry, examples of actual over-temperature effects on material at a microstructural level may be considered proprietary and publication of these results is limited. It is therefore difficult to obtain micrographs of actual blade samples having experienced short-term overtemperature, illustrating whether significant change in volume fraction of the precipitate has occurred.

The following thesis includes description of a series of experiments designed to provide quantitative results showing the effects of temperature, time and basic tensile loading on a directionally-solidified, nickel-based superalloy, Rene 80, representative of material commonly used in turbine blades. The experimental procedure which involves "simulated" short-term overtemperature using a Gleeble thermo-mechanical apparatus is described in Chapter 3. Simulated thermo-mechanical testing is achieved by applying a programmed load to the specimen, resulting in a controlled temperature increase of the material that can be recorded. Results of the experimentation are described in terms of the achieved heating profile, and also through metallurgical evaluation of the ratio of precipitate to matrix. Differences in volume fraction of gamma prime to gamma ($\gamma$':$\gamma$) and changes in morphology of the metallurgical samples are presented and discussed in the following chapters, including potential theories to support experimental results. Chapter 5 summarizes these data and theories, highlights limitations of the current study and contains suggestions for potential future research.

# Chapter 2

# Literature Review

## 2.0 Introduction

The literature review begins with an overview of the characteristics and properties of nickel-base superalloys including description of the basic physical metallurgy of Rene 80 DS, the directionally solidified nickel-based superalloy used in the experimental portion of this thesis. An overview of the mechanics of diffusion, which is the process by which the gamma prime precipitates are dissolved into gamma matrix is then presented. A review of available research on the microstructure of blade materials is included to illustrate the emphasis of research mainly reflecting long-term effects. Definitions and relevance of the condition of "short-term overtemperature" are then addressed, followed by justification for attempting to report a quantified evaluation of gamma prime to gamma phase volume fraction. This chapter concludes with statements regarding the scope and objective of the current work.

## 2.1 Physical Metallurgy of Rene 80

### 2.1.1 Overview of Superalloys

Nickel-based superalloys are understandably composed primarily of nickel, usually to approximately 60% by weight, with additions of chromium and cobalt in the next highest constituents, and additional elements in ranges of less than 0.1% up to nearly 10% by weight. Each alloying element contributes to serve varying functions such as improving corrosion resistance, increasing melting point of the alloy, improving solubility of other elements, and

assisting in formation and stability of precipitates. Ni-base superalloys typically consist of a two-phase system whereby an intermetallic precipitate is formed from a solid solution matrix of gamma phase (γ) to offer the material its main source of strength. The precipitate phase, known as gamma prime (γ'), is a highly ordered $L1_2$ intermetallic constituent of composition $Ni_3$(Al, Ti, Ta), with a face-centered cubic crystallographic structure. The γ matrix is the austenitic (also FCC) phase of nickel and although it is often represented as pure Ni, does contain the other alloying elements.

The alloys can be heat-treated to optimize the volume fraction of gamma prime precipitate to the gamma phase matrix (γ':γ), by holding the material for several hours at a temperature within the range conducive to formation and growth of γ'. This heat treatment is often called a precipitation heat treatment (PHT), and the resulting materials are known as precipitation hardened or precipitate hardenable (PH) alloys. [4, 5, 6] Morphology of the precipitate phase can range from spherical, to cuboidal, to cubic, and morphology is strongly influenced by the elemental content of aluminum and titanium. Cubic γ' are characteristic of an alloy containing more Al than Ti; whereas a higher content of Ti than Al tends to yield more spherical γ'. It is also possible to obtain systems containing a dual morphology, such as a primary cuboidal γ' surrounded by finer, secondary γ' which are typically spheroidal. [5]

The resulting combination of alloying elements and post-casting thermal manipulation of the microstructure results in a class of materials that is well-known to perform reliably under conditions of temperature cycling up to 80% of their melting points, load cycling and in environments of corrosive gases. Nickel-base superalloys are able to maintain their strength within these harsh conditions largely due to the presence and thermodynamic stability of the precipitate phase, which is the primary topic of study in this thesis. [1-8]

### 2.1.2 Directionally Solidified Rene 80

#### 2.1.2.1 Directional Solidification

Rene 80 is a nickel-base superalloy, trademark of General Electric, typical of the parent material used in gas turbine blade production. For turbine blades, the alloy is produced from vacuum melted investment castings, where cooling is controlled to form aligned material grains resulting in what is known as directionally solidified material. [2, 4] Because grain boundaries are regions differential in free energy from intragranular regions, entities such as carbides and other constituents will form there preferentially upon cooling. It is well-known that grain boundaries and their characteristics can have strong effect on the mechanical properties of superalloys. During their early development, production of superalloys evolved from castings of amorphous polycrystalline structures to structures of directionally solidified crystals yielded by controlled cooling. It was considered desirable for a component such as a turbine blade to contain like-oriented grains, whose boundaries perpendicular to the principal direction of loading had been eliminated in order to eliminate the easiest path of fracture. In a turbine engine, the principal load acting on a blade is considered to be radially outward from the axis of rotation, or a tensile load from blade root to tip. [7] Orienting grain boundaries to coincide with this principal load was thought to maximize utility of grain boundary strength in part due to the presence of globular-type carbides that form in or along grain boundaries, while providing enough ductility to respond to principal loading in service. [5, 7, 8] In 1976, Nakagawa et al. [9] published their study comparing conventional cast Rene 80 to DS cast samples and found improvements of 10 – 15% in yield strength and tensile strength at temperatures from 600 – 980ºC for directional solidification over conventionally cast Rene 80. The authors credit mechanical improvements to directional alignment of crystals and absence of grain boundaries perpendicular to principal

stress. Although producing material of a single crystal became possible alongside development of DS alloys, initially, the benefits to mechanical properties of single crystal were not significant over those of DS materials compared to the extra cost to produce. Eventually, the process for obtaining single crystal alloys was also refined and it is now common to encounter components without any grain boundaries at all. [7, 8]

#### 2.1.2.2 Composition and Role of Alloying Elements

As stated earlier, different elements are added to an alloy system for a variety of reasons that contribute to improving the properties of the material. Each element's physical properties such as atomic size, mass, melting point and density, will contribute to the overall characteristics of the alloy. Purpose of an alloying element can range from improving corrosion resistance, to raising or depressing melting point of the alloy, to assisting in formation or behaviours of the γ' second phase or carbides. Elements often fulfill multiple roles. Table 2.1 contains the nominal elemental composition of conventional cast Rene 80 and DS Rene 80Hf (with halfnium) per the Non-Ferrous Alloy composition tables within the ASM Handbooks. Table 2.2 contains a summary of which alloying elements fulfill which roles.

**Table 2.1: Nominal compositions of directionally solidified Rene 80 by wt% [10]**

| Alloy | Co | Cr | Mo | W | Ta | Re | Ru | Nb | Al | Ti | Hf | C | Zr | B | Ni |
|---|---|---|---|---|---|---|---|---|---|---|---|---|---|---|---|
| Rene80 | 9.5 | 14.0 | 4.0 | 4.0 | | | | | 3.00 | 5.0 | | 0.170 | 0.030 | 0.015 | bal |
| Rene80 Hf | 9.0 | 14.0 | 4.0 | 4.0 | | | | | 3.00 | 4.7 | 0.80 | 0.160 | 0.010 | 0.015 | bal |

**Table 2.2: Summary of alloying elements and their roles [11, 12, 13]**

| Effect | Alloying elements |
|---|---|
| Solid solution strengtheners | Co, Cr, Fe, Mo, W, Ta, Re, Ru, Al |
| Forms MC carbides | W, Ta, Ti, Mo, Nb, Hf |
| Forms $M_{23}C_6$ carbides | Cr, Mo, W |
| Forms $M_6C$ carbides | Mo, W, Nb |
| Forms $\gamma'$ $Ni_3$ (Al, Ti) | Al, Ti, Ta |
| Raises solvus temperature of $\gamma'$ | Co, Mo |
| Hardening precipitates and/or intermetallic | Al, Ti, Nb |
| Oxidation resistance | Al, Cr, Y, Si, |
| Improves creep properties | B, Ta |
| Retards $\gamma'$ coarsening | Re, Fe, Co, Mo, Nb, Ti |

For Rene 80, the main γ'-formers are aluminum, and titanium, with Al being present in a slightly lower content than Ti (3.0 Al, 5.0 Ti). Tantalum is a precipitate-forming element commonly added to nickel-base superalloys, but it is not present in Rene 80. The addition of Al and Ti is relatively small because aside from adding benefit to the alloy by forming the main strengthening phase, Al and Ti can be embrittling agents, and melting point depressants. [2, 12] Chromium, cobalt and tungsten may also be considered precipitate formers and may be present in precipitates. However, the primary function of Cr is to provide corrosion resistance at high temperatures, and Mo and W provide solid solution strengthening. Boron and zirconium are added in minute amounts and contribute to creep rupture properties. [8] Individual elements may also subtly influence characteristics such as unit-size of γ' and solution temperature of these second phase constituents. The effects of composition on the characteristics of γ' are discussed in greater detail in later sections of this thesis.

Aside from γ' precipitates, the other constituent of significance is the presence of metal carbides. Carbon has an affinity to formation of carbides with Cr in particular, but also with many of the other elements (Co, Mo, Ti, W, and Zr) and may be present as MC, $M_{23}C_6$, or $M_6C$ (where M is representative of a metallic element) depending on the heat treatments the material has undergone. Upon initial cooling of the castings, the most common form of carbide in Rene 80 is MC. Subsequent heat treatments will induce an evolution of carbides either to solution and then reprecipitate or to break down into $M_{23}C_6$ or $M_6C$. As mentioned earlier, carbides are usually globular in appearance, larger in size (up to 200 μm) than typical γ' precipitates and tend to form at or along grain boundaries. [1, 2, 5, 8, 14] These elements, most likely to form carbides, may then be considered grain boundary strengtheners. Figure 2.1 shows various carbide precipitates found in Rene 80 and the corresponding temperature ranges through which they are present.

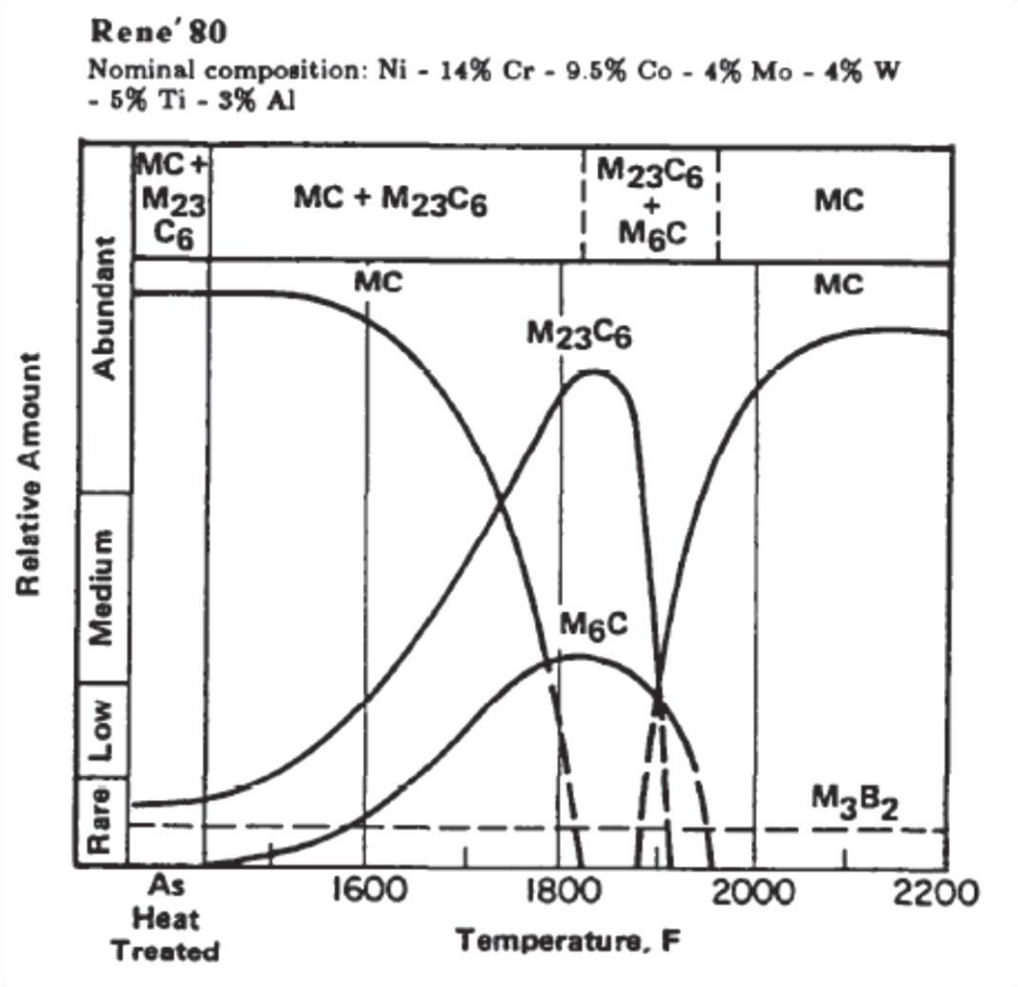


**Figure 2.1: Occurrence of carbide precipitates relative to temperature. [15](Reprinted with permission)**

It may be noted that following prescribed heat treatment, mainly MC-type carbides are present with some $M_{23}C_6$, but that at higher temperatures (1825–1900 ºF, or ~1000–1035 ºC), representative of those seen in service, the MC carbides have transformed to larger occurrence of $M_{23}C_6$ plus some $M_6C$. It is also apparent that metal borides may be present throughout the entire range of temperatures shown, but that their occurrence is rare.

The chemical interaction of alloying elements and their effects on mechanical properties and behaviours of the superalloy at high temperatures and under load are a complicated topic. The purpose of this section is to provide only a basic understanding of the significance of particular elements over others and to illustrate that each element is present in the alloy for a reason.

### 2.1.3 The Gamma Prime (γ') Phase

The gamma prime precipitate phase is arguably the most essential aspect of Ni-based superalloys and it has been studied in great detail. In their review of the microstructure of Ni-base superalloys, Sullivan and Donachie Jr. report a list of conditions that will ensure a precipitate is effective as a second phase. [8] The conditions include a minimum volume fraction of 30% gamma to gamma prime (γ':γ), recommendations on interparticle spacing of the precipitates, a requirement that γ' should exceed strength of the γ matrix but still exhibit enough ductility to prevent fracture, and that the interface between precipitate and matrix be coherent to ensure stability. [8]

#### 2.1.3.1 Volume Fraction of γ'- γ

Volume fraction can be controlled to some degree through regimented heat treatments conducted on the material after initial casting and after any additional precision machining has been completed, but prior to service. The heat treatment can produce with repeatability a desired

average size of γ' precipitates as well as yield an overall volume fraction of γ':γ within a particular range, because temperature and time of heat treatment both affect nucleation and growth of the γ' phase. For Rene 80, the gamma prime precipitates begin forming during cooling at a temperature of approximately 1156 ºC. [12] The regime for precipitation heat treatment begins with holding the material at a temperature high enough for all constituents to dissolve into solution, and provide homogenization of the material. This solution and homogenization temperature is usually in the range of 1100-1250ºC depending on the alloy (T > 1200ºC for Rene 80) and time at temperature may also depend on thickness of the material, although 2 - 4 hours is typically sufficient. Temperature is then reduced to a range conducive to γ' precipitation (800 – 1100 ºC) and either held for a long period of time, or further reduced to incur secondary precipitation and held at the second temperature. This stage of heating is known as "aging". The aging cycle can be anywhere from 12 – 24 hours. Its purpose is to allow for thermodynamic stabilization of the γ'-phase, which, in practical terms, results in uniformly sized and shaped particles, uniformly dispersed within a continuous matrix. For two step aging processes, a bi-modal structure of primary (larger) and secondary (smaller) γ' precipitates would be achieved. Inter-particle spacing is dependent on the size of precipitate and on the resulting volume fraction. In turbine blade applications, superalloys are produced to consist of a system of greater than 50% volume fraction of γ': γ, and for Rene 80, heat-treated to produce uniformly sized γ', the cuboidal particles may average 0.3 – 0.5 μm in size. [1, 6, 14, 15, 16]

#### 2.1.3.2 Coherent Interface of γ'- γ

Coherency of the precipitate and matrix, and strength of the γ' precipitate are inter-related characteristics, the understanding of which requires review at the atomic level. The ordered cubic lattice of $Ni_3(Al,Ti)$ γ' precipitate phase is high in symmetry, and precipitates naturally in a

coherent manner to the matrix lattice. Representations of the two phases are shown in Figure 2.2 Coherent refers to the close dimensional relationship between lattices of the matrix and precipitate at their interface. Gamma prime will have a unit cell lattice parameter, $a_0$, of approximately 3.5 – 3.6 Å, depending on whether it forms with Al or Ti. For the nickel matrix, $a_0$ is often approximately 3.56 Å. [4, 5, 17] These similar values of $a_0$ for γ and γ' result in a small amount of lattice strain at the interface. The small difference in lattice parameters is called mismatch or disregistry (δ) and can be a negative value depending on whether the matrix or the precipitate has the larger size. The degree of mismatch contributes to the resultant morphology of γ' precipitates. Upon initial cooling, when γ' is first nucleating and mismatch is extremely close to zero (0 -0.2%), precipitates will appear spheroidal. As strain between lattices at the interface increase (0.5 – 1.0%), still a coherent interface but with strain, the precipitate takes on a more cuboidal shape. [16, 18] Given that strain exists between adjacent atoms of γ and γ', it is easy to make the connection to an increase in interfacial energy, and thus understand that mismatch also has an effect on precipitate strength. Also, because the lattice parameter changes depending on whether the γ' composition is $Ni_3Al$ or $Ni_3Ti$, it is understandable that overall content as well as local concentration of Al and Ti, will influence mismatch and thus properties of the precipitate. This is a topic of interest in the current work: atomic mismatch, and its potential to influence the persistence or dissolution of gamma prime will be discussed further in later sections.

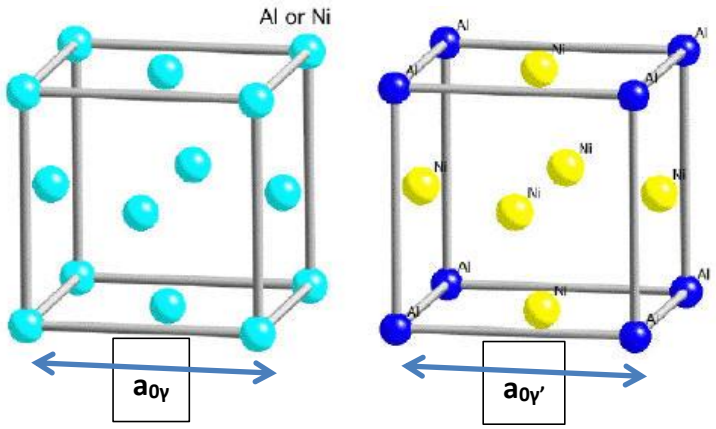


**Figure 2.2: Graphical representations of FCC nickel (Gamma) and $Ni_3Al$ (Gamma-prime) [19]**

### 2.1.4 Dissolution of Gamma' (γ')

When a material is held within a specific temperature range upon cooling from temperatures above the solution point, precipitation of γ' from the super-saturated matrix will result. When the same material is heated through a similar temperature range, the γ' precipitates will dissolve back into solution. Under conditions of slow heating rate (2 ºC/minute), the bulk of γ' precipitates in a material will dissolve at a singular temperature, referred to as the γ' solvus temperature. Complete dissolution of all precipitates is possible at this temperature. Determination of γ' solvus for a particular alloy requires rigorous experimentation due to dissolution of γ' depending not only on temperature alone, but also on many other factors. Dwell time at temperature, heating rate, initial volume fraction of γ':γ', precipitate size and concentration of elements are all factors that may influence dissolution. [12, 20] In his summary of differential thermal analysis of varying superalloys, Sponseller articulates that the temperatures to represent dissolution of γ' will vary with the reaction type, but that the relationship will tend to the same trend. Specifically, the precipitation reaction upon cooling,

will produce a lower γ' solvus than for the dissolution reaction upon heating, and the equilibrium γ' solvus will lie in between.

$$T_{\gamma' \text{ solv, cooling}} < T_{\gamma' \text{ solv, eqm}} < T_{\gamma' \text{ solv, heating}}$$

For DS Rene 80, the "practical" dissolution temperature of γ' ($T_{\gamma' \text{ solv, eqm}}$) is designated as 1150ºC, whereas the γ' solvus on cooling (precipitation reaction) has been reported as 1156 ºC. [4, 12] Although these values are not in agreement with the relationship laid out by Sponseller, the temperatures are reported as "approximate" in the case of $T_{\gamma' \text{ solv, eqm}}$ and "average" for the results of Sponseller's DTA experimentation. In the current work, the value of $T_{\gamma' \text{ solv, eqm}}$ = 1150 ºC is observed and utilized in analysis.

In general, the process of precipitate dissolution may occur in either of two modes, depending on the heating conditions: a) solid state dissolution, or b) liquid state dissolution. The mechanisms that drive these two modes of dissolution are different, and are discussed in the next sections.

#### 2.1.4.1 Solid State Dissolution

Solid state dissolution of a precipitate involves two atomic processes, dissociation of atoms from the precipitate and migration of the atoms into the matrix. Atoms must first have enough energy to dissociate from the precipitate, and will then migrate into the matrix in pursuit of a lower state of energy, or higher state of stability. [18] As heat increases, solubility of the γ' forming elements in the matrix increases, and Al and Ti atoms (for Rene 80) will leave the precipitate and enter solution within the matrix. While these two atomic processes occur, the interface between precipitate and matrix gradually migrates toward the center of the precipitate, causing it to reduce in size. The process of migration of atoms may also be called diffusion. Solid state dissolution may then be described as a thermally-activated, diffusion-controlled phase

transformation during which atoms are migrating from the precipitate to the matrix lattice. When a system is allowed sufficient time to achieve thermodynamic stability at the γ' solvus temperature, diffusion will occur in a repeatable manner, predictable by using Fick's Laws and empirical data specific to the alloy, and the bulk of precipitates will dissolve into solution with the matrix. These conditions of thermodynamic stability may be said to represent equilibrium for precipitate dissolution. In practice, equilibrium solid state dissolution tends to be observed during regular heat treatments where the alloy is heated within a vacuum furnace at a controlled (slow) heating rate, allowed to dwell at a constant temperature for a long period of time, usually under conditions of no applied load. [18, 20]

Any departure from these type of conditions may be referred to as non-equilibrium. Given that for practical applications, this may be considered the more common environment, it is worth understanding changes in behaviour of the material. As stated earlier, Sponseller found that the γ' solvus temperature can vary with reaction type (on-heating versus on-cooling) and with heating rate. Soucail and Bienvenu conducted a study of dissolution of the γ' phase under equilibrium conditions and compared to conditions of rapid heating. [21] Their findings agree with Sponseller; specifically, they found that the γ' solvus temperature increased with increasing heating rate, and that the degree of change from equilibrium in peak temperature of dissolution was dependent on initial size of the precipitate, where a larger initial radius produced a more significant differential in peak dissolution temperature. [12, 21]

#### 2.1.4.2 Liquid State Dissolution

Studies of dissolution under non-equilibrium conditions have been used to observe changes in the maximum temperature of complete precipitate dissolution, and have confirmed that heating

rate, dwell time and precipitate size will influence the dissolution process. Researchers have also discovered that there is a limit to the capability of the second phase to dissolve via solid state transformation. Because solid state dissolution is ultimately dependent on the diffusion capabilities of the solute atoms (Al, Ti), time is required for diffusion to proceed. In cases where heating rate is rapid and dwell time is brief, it is possible for dissolution to occur by liquid phase transformation. As indicated in the former section, second phase dissolution involves two atomic processes, dissociation of atoms from the precipitate and migration of the atoms from precipitate into the matrix. Sufficient energy and sufficient time are both required for completion of solid state dissolution, and in cases where heat input occurs at or beyond a critical rate, coupled with brief dwell time at peak temperature (sufficient energy, but insufficient time), γ' precipitates will dissolve by process of constitutional liquation rather than solid state dissolution. [22]

In 1967, Pepe and Savage published an article explaining the process of constitutional liquation of second phase particles. The article uses a theoretical binary phase diagram to support their presentation of progression of phase transformation, shown in Figure 2.3 for reference. [22] It also contains schematic representations showing the progression of the concentration gradient across the particle to matrix interface. In Figure 2.4, the initial scenario depicts a solid-solid precipitate-matrix interface (at $T < T_{eutectic}$) corresponding to $T_3$ in the phase diagram in Figure 2.2. As the particle radius of the solid precipitate reduces, an inside interface of solid precipitate to liquid film of matrix high in solute concentration is formed, and a second interface to solid matrix exists (at $T = T_{eutectic}$). As temperature further increases to a point corresponding with $T_4$ in Figure 2.2, the particle further reduces in radius of solid precipitate, interfaces to a band of liquid phase and exhibits a second liquid-solid matrix interface (at $T > T_{eutectic}$).

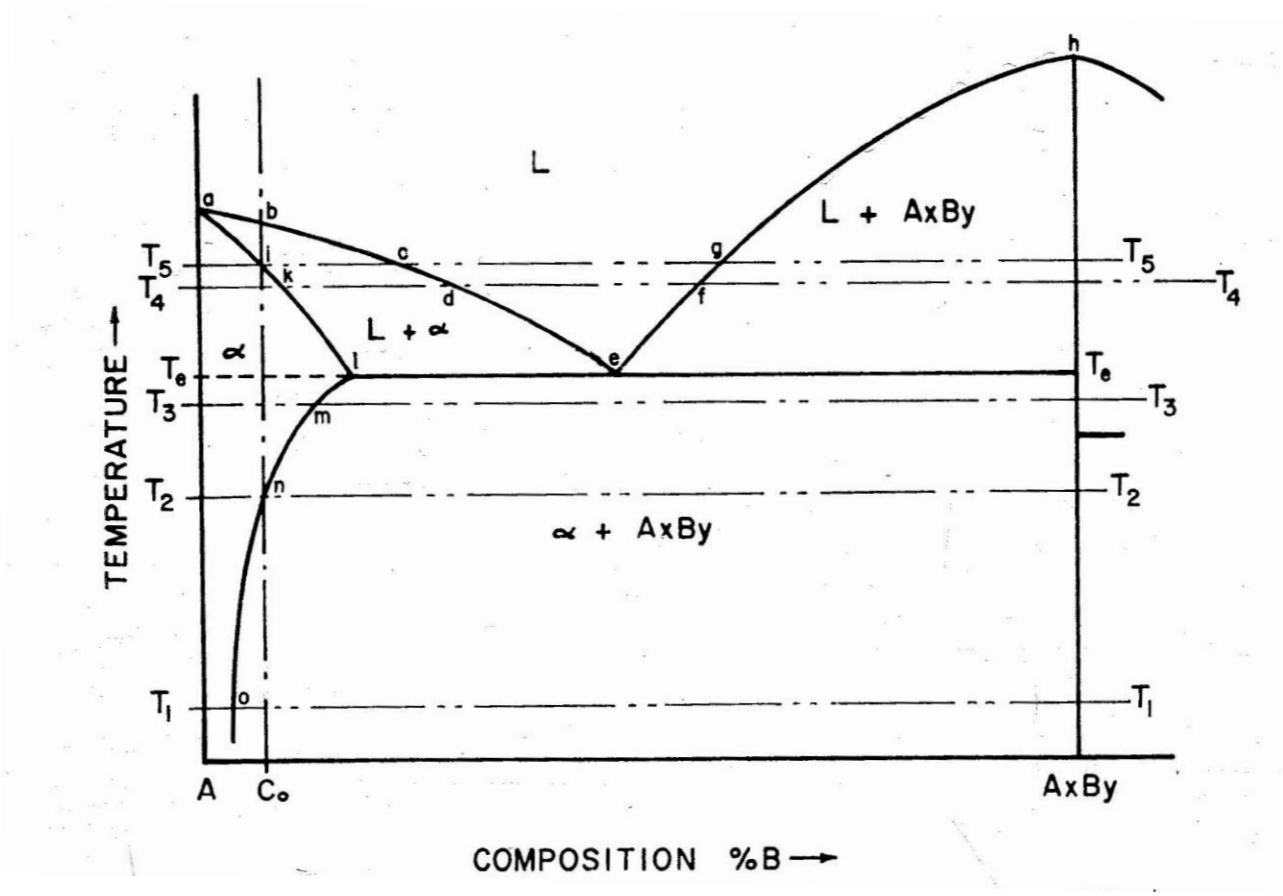


**Figure 2.3: Hypothetical binary phase diagram used to illustrate constituional liquation. [22]**
(reprinted with permission from the Welding Journal, American Welding Society)

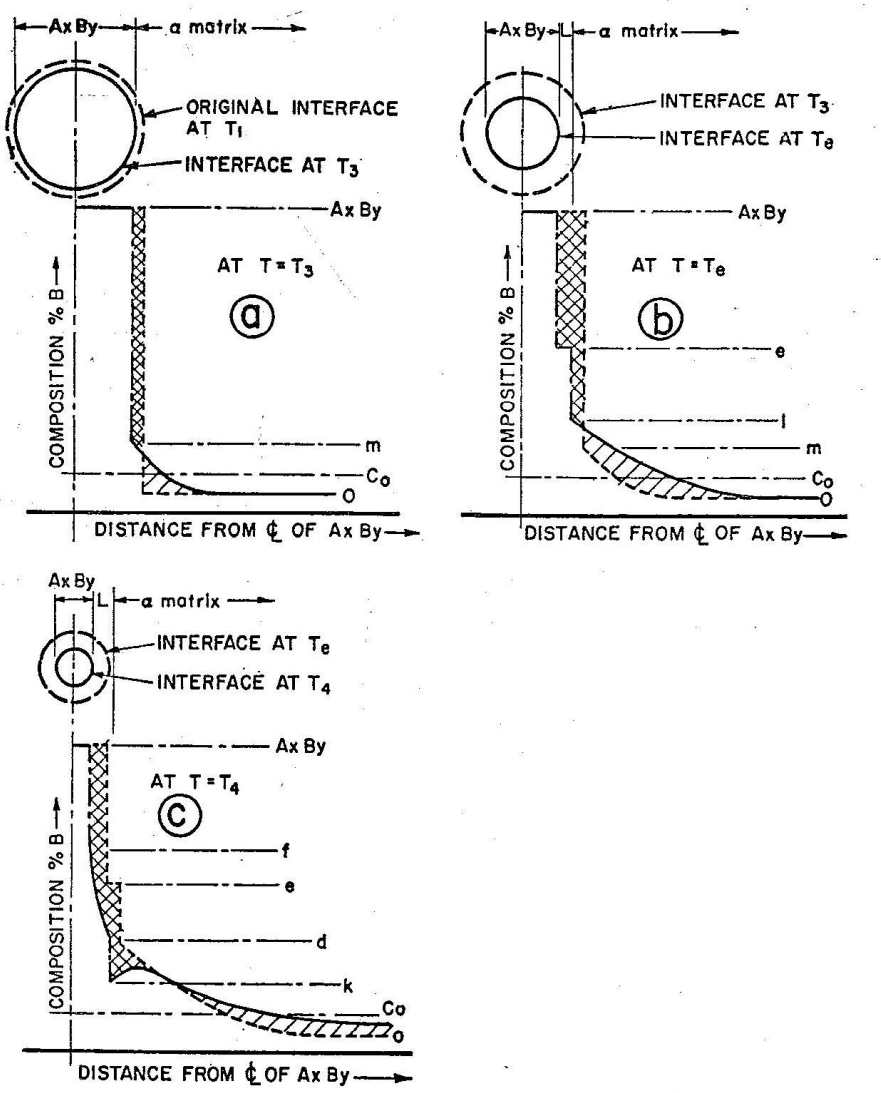


**Figure 2.4: Graphical representation of progressive concentration gradients across particle-matrix interface during constitutional liquation. [22]** (reprinted with permission from the Welding Journal, American Welding Society.)

In the final stage of transformation, temperature is above the eutectic for a specific composition, but below the equilibrium solidus of the alloy. Due to extreme concentration gradients across the interfaces with rapidly changing temperature, the material responds with a eutectic-like reaction that results in formation of the liquid film between solid phase precipitate and solid phase matrix. [22, 23, 24]

## 2.2 Diffusion

Whether dissolution of gamma prime precipitates is occurring by solid or liquid state dissolution, the principles of diffusion must be understood in isolation of the atomic processes involved with dissolution of the second phase. Diffusion is the migration of atoms through a material over time. In the following section, the basics of steady-state and non-steady state diffusion, kinetics of diffusion and theories surrounding strain-assisted diffusion are introduced.

### 2.2.1 Fick's Laws

Steady state diffusion can be described by Fick's first law, and occurs under isothermal conditions over a period of time. Fick's first law states that a diffusive flux will vary with a magnitude proportional to the concentration gradient. [25, 26] This expression implies that concentration is the main driving force behind the movement of atoms. It relates concentration to distance where the reaction is proceeding at a constant temperature. It may be represented as follows:

$$J = -D\frac{dC}{dx} = -D\frac{\Delta C}{\Delta x} = -D\frac{(C_2 - C_1)}{(x_2 - x_1)} \qquad \text{(eq. 2.1)}$$

where J is the diffusion flux, D ($m^2/s$) is the diffusivity constant for the material, C and x are concentration and distance. This first law is effective in describing conditions of diffusion where the concentration gradient is assumed to be linear. It is adequate in representing the penetration of atoms of a single species through a finite distance (one dimension) at a continuous temperature and is typically used to represent simple applications where diffusivity constant is already known. One such example may be calculating the time required at a given furnace

temperature for carburization of a component of uniform composition to a desired depth from the surface.

Fick's second law allows for a curved concentration profile, which is more practical than a linear profile for many situations, and requires a partial differential equation to describe diffusion.

$$\frac{\partial C}{\partial t} = D\frac{\partial^2 C}{\partial x^2} \qquad \text{(eq. 2.2)}$$

Mathematical solutions of this equation involve use of the Gaussian error function, and account for varying concentration gradient with respect to time and to distance, or a non-steady state diffusion condition. [25, 26] This approach may also be used to solve relatively simple diffusion problems. Using the carburization example, Fick's second law would be used potentially to predict length of time needed at a given temperature to achieve a specific concentration of carbon within the substrate at a specific depth. Although frequently used to approximate non-steady state conditions, this approach still has limitations in that it requires constant pressure and temperature and assumes the diffusivity constant is known and is independent of composition. [25, 26, 27]

The diffusion coefficient, D, is an expression of the rate at which a species of atoms will diffuse. It may be defined using the following Arrhenius equation:

$$D = D_0 \exp\left(-\frac{Q}{RT}\right) \qquad \text{(eq. 2.3)}$$

where $D_0$ is the pre-exponential constant specific to the material, Q is the activation energy required for the process to initiate, R is the gas constant and T is temperature in absolute form. The pre-exponential diffusion constant, $D_0$, is a function of atomic characteristics unique to the

material such as frequency of jump attempts, and lattice parameter, and also contains geometric and correlation factors dependent on the crystal structure. [26, 27] The three equations described above are the most basic mathematical representations of diffusion. In order to account for the complexity of atomic processes for phase transformation such as precipitate dissolution, one has to consider more than just the basics of diffusion described by Fick's Laws. Study of the kinetics of transformation is another important aspect which is discussed next.

### 2.2.2 Kinetics of Phase Transformation

Although diffusivity is represented mathematically by a constant, it must be noted that phase transformation processes do not typically proceed at a constant rate. Diffusion limited phase transformations have been analyzed and found to adhere to empirical rate equations. Rate of phase transformation of a dissolving precipitate typically follows a sigmoidal curve where rate of reaction is slow at the beginning and at the end of transformation. [18, 28] Rate is dependent on the thermodynamic properties of the system (activation energy, Q) and also on extent of the reaction. Jena & Chaturvedi relate the empirical rate equation to a function of the fraction of transformed material, Y, through the below equation. [18]

$$\left(\frac{dY}{dt}\right) = [f(Y)]k_0\, exp\left(-\frac{Q}{RT}\right) \qquad \text{(eq. 2.4)}$$

From the above equation, $f(Y)$ describes only the function of fraction-of-transformation, and the temperature dependence of the reaction rate is defined by a rate constant, k, which represents the exponential portion of the reaction such that

$$\mathrm{k} = k_0\, exp\left(-\frac{Q}{RT}\right) \qquad \text{(eq. 2.5)}$$

If Y is the fraction of transformed material, then 1-Y equals the remaining untransformed material. The rate equation used to describe sigmoidal-type kinetics is then a function of Y and (1-Y):

$$\left(\frac{dY}{dt}\right) = Y^m (1 - Y)^r k \qquad \text{(eq. 2.6)}$$

where *m* and *r* are constants whose values can be determined experimentally. When the progress of reaction is plotted against log time, a series of sigmoidal curves will be obtained, where each curve represents an isothermal reaction at a different temperature. Significant experimentation is required to produce this type of data for a reaction of one type. Using the experimental data to establish a new dataset of times to achieve a constant fraction of transformation is one method that may be used to obtain a value for activation energy. Plotting the natural log of the time values versus the inverse absolute temperature should then yield a linear relation whose slope may be used to calculate a value for activation energy, Q. Obtaining a calculated value for the activation energy required for a specific phase transformation is useful in understanding the atomic mechanism behind the diffusion process, since the activation energy will be different depending on whether diffusion is occurring by vacancy, by substitution or by interstitial mechanism, and where interstitial mechanism is typically a lower value of Q than vacancy mechanism in the same system. [18, 26, 27, 29]

Mathematical modelling of diffusion processes generally involves the use of a form of Arrhenius equation. In the early 1970s, controversy surrounded the application of kinetic theories to approximating the process of precipitate dissolution. Initially, it was assumed that dissolution may be considered to be the reverse process to growth. As researchers worked to validate theories experimentally, different approximations were studied, considering single dimension,

planar and finally spherical models to represent diffusional reduction in size of theoretical precipitates. The theories for mathematical modelling also considered invariant field, invariant size (stationary interface), linearized gradients and reversed growth, all in attempts to simplify some aspect of the diffusion expression. Eventually, some agreement on components of the mathematical approximations were reached, the basics of which are presented next. [28, 30, 31]

For dissolution, the dependence of diffusion on time may be reduced to the following equation showing change in square of the particle radius with time:

$$dR^2/dt = -kD \qquad \text{(eq. 2.7)}$$

*R* is the particle radius, *D* is the diffusion coefficient, and *k* is a constant representing the relationship between solute concentration in the precipitate, in the matrix and at the interface. [28, 30]

As a diffusion-controlled process, solid state dissolution requires time for transforming to fruition from one phase to another. Because precipitate dissolution is a complex phase transformation whose overall rate can depend on many characteristics of the material in localized areas (composition of the precipitate, the surrounding matrix, the presence and degree of strain at the interface, for example), analytical models representing the kinetics are also complex. Researchers have proposed that for dissolution, transformation is dependent on two components of diffusion: a) steady state and b) transient, where the transient diffusion component has a stronger effect and contributes to more rapid rate of dissolution at the initiation of dissolution (shorter times) versus toward completion of particle dissolution. In this context, "steady state" refers to conditions when diffusion flux (J) in the matrix is equal to flux of the interface ($J\gamma = J_I$),

and “transient” represents conditions of flux inequality. [28, 32] These concepts are discussed with greater detail following presentation of results of the current study in Chapter 4.

### 2.2.3 Strain-assisted Diffusion

Similarly to Whelan’s assertion that dissolution is truly represented by a component of steady state diffusion plus the transient component of diffusion that changes with changing precipitate size, so have there been models that consider the effect of lattice strain to contribute to the kinetics of dissolution. The basics of diffusion use concentration gradient to describe diffusion flux because in many systems, concentration as a driving force contributes more strongly than other forms of energy. However, it is also well known that diffusion can still proceed in cases where concentration gradient is zero. External driving forces such as an electrical field, temperature gradient (discussed earlier), stress gradient, and even gravitational or centrifugal forces have been proven to influence diffusion. [26] In the study of nickel-based superalloys used in turbine blade application, the potential effect of a stress gradient is of particular interest, given that blades are subject to complex loading during operation.

Given the strong effect of temperature on activation energy, and thus diffusivity, and given the strong effect of concentration gradient as a driving force behind diffusion, isolating the effects of stress (and therefore strain) can be challenging. Cowern et al [33]were able to conduct experiments that showed an exponential increase in diffusion due to strain by observing the diffusion of germanium solute through a silicon matrix. Through diffusion simulation in states of unstrained and strained material, they were able to show activation energy, *Q*, as a function of strain, *s*, where the following linear relationship holds:

$$Q(s) = Q(0) + Q's \qquad \text{(eq. 2.8)}$$

where $Q' = dQ/ds$, representing the activation energy of diffusion per unit strain, $s$. [33]

They also found experimental data to correlate well with the following Arrhenius expression relating diffusivity in strained material, $D_{strain}$ to the corresponding diffusivity in unstrained material, $D_{unstrained}$:

$$D_{strain} = D_{unstrained} exp\left(\frac{-Q's}{kT}\right) \quad \text{(eq. 2.9)}$$

where $Q'$ and $s$ are the activation energy per unit strain and strain respectively and $k$ represents a constant. This increase in diffusivity requires the strain to be compressive, because the analysis involves sign such that a negative strain (compressive) changes the exponent to a positive value resulting in a stronger effect. However, other studies of diffusion in the presence of strain are not sign specific in this manner. Antonelli and Bernholc computed the energies of formation of vacancies in silicon as a function of pressure and found a linear decrease in the energy of vacancy formation with increasing strain. [34] A linear reduction in energy of formation implies a corresponding reduction in activation energy of diffusion provided the mechanism of diffusion is vacancy dependent. Cowern also suggests that a tensile strain could enhance diffusion if the dominant mechanism of diffusion were interstitial as opposed to vacancy. [35] In general, it has become an accepted theory that stress can be a driving force in atomic migration and therefore influence both the onset and overall rate of diffusion. [33, 34, 36]

## 2.3 Overview of Turbine Blade Literature

The most common conditions for removal and replacement of turbine blades are excessive wear, corrosion, erosion, and life limit exceeded. Given the known extreme environment of high

temperature and corrosive gases, many studies have been conducted researching the behaviour of nickel-base superalloys over long periods of time (on the order of thousands of hours) in order to understand turbine blade materials' response to long term effects of conditions such as creep and fatigue, both of which may lead to ultimate failure of the blade material. [1, 37] Understanding the aspects surrounding creep and fatigue, which are both potential modes of eventual failure of a blade operating under "normal" conditions is of course essential in setting component limitations that ensure flight safety. References analyzing the onset and progress of creep and fatigue are easily obtained for nickel-based superalloys representative of blade materials. [1, 25, 29, 37]

Although a common area of study of nickel superalloys, and a common condition of turbine blade failure, fatigue is included here only superficially. Fatigue is a phenomenon which can drive the initiation and propagation of cracks as a result of repeated cycles of loading and is an essential topic in understanding the behaviour of blade materials in engine operation. However, the atomic processes involved in crack initiation and propagation are complex and involve theories not analyzed in greater detail within this thesis. It is listed as an example of a mechanical failure mode that is a topic of significant research in blade materials, but which lies outside the scope of this research.

### 2.3.1 Long-term Coarsening

Long-term exposure of precipitation-hardened nickel superalloys to temperatures below the dissolution temperature of gamma prime results in a phenomenon known as Ostwald ripening. Larger γ' particles grow in size at the expense of smaller particles which will dissolve in order to reduce the overall energy of the system. The driving force behind coarsening, which is a

diffusion-based process, is decrease in the total surface free-energy. Since the temperature range required for coarsening is moderately lower than γ' solvus, it typically coincides with engine operating temperatures. As a result, Ostwald ripening is a microstructural condition normally present in turbine blades after hundreds of hours of service. [38, 39]

Quantitative theories to describe the growth kinetics of gamma prime particles have been presented and analyzed for close to fifty years. In 1970, Ardell published a study on growth of $Ni_3Ti$ γ' particles, that correlates experimental data to the Lifshitz-Wagner model of diffusion-controlled coarsening. [40] At the time, the conclusions offered proof that growth was a diffusion-controlled mechanism for $Ni_3Ti$ γ'-particles, now a widely accepted premise. Shortly after this publication, a variation of the L-S model, known as the LSW (Lifshitz-Slyosov-Wagner) became the standard to which other models were compared. [38, 40] In more recent years, researchers have attempted to assert whether kinetics adhere to cube- or square-rate laws. In their study of long-term aging, Hadjiapostolidou & Shollock used Rene 80 to compare two mechanisms for growth:

1. Diffusion-controlled particle growth described by the cube rate law,

$$r_{avg}^3 \propto k_1 t$$

where $k_1$ is a diffusion-controlled constant and $r_{avg}$ is the average particle radius at time, $t$, and,

2. Interface reaction-controlled growth described by the square rate law,

$$r_{avg}^2 \propto k_2 t$$

where $k_2$ is an interface-controlled constant and $r_{avg}$ is the average particle radius at time, $t$. [41]

Analysis of the rate controlling mechanisms yielded inconclusive results in that coarsening was found to fit better to the cube rate law under some conditions and fit better to the square rate law under some conditions. The authors reported that for Rene 80 at aging temperatures of 850ºC and 900ºC, experimental data fit better to the cube rate law for all aging times, but for higher temperatures of 950ºC and 1000ºC, the square rate law produced a better fit to data. In addition, at a temperature of 950ºC, the cube rate law fit better to data for shorter aging times (up to 2000 hours) and the square rate law to the longer times (2000 – 20 000 hours). They concluded that neither interface-controlled mechanism (square rate law) nor the diffusion-controlled mechanism (cube rate law) could be considered the dominant mechanism based on results of their experiment. This statement contradicts other research, where coarsening was reported to follow cube rate law (diffusion control) more dominantly than square rate control. [32]

For each of the two mechanisms, the constant, $k_1$ *or* $k_2$, is temperature dependent and the following relationships hold.

$$k_1 T \propto exp\left(\frac{-Q}{RT}\right)$$

$$\ln(k_1 T) \propto \text{constant} - (\frac{Q}{R})(\frac{1}{T})$$

Activation energy, Q, can then be calculated by plotting experimental values of $\ln(k_1 T)$ versus 1/T. The calculated value for coarsening activation energy reported by Hadjiapostolidou et al. is Q = 127 kJ/mol. [41] This is significantly lower than the value of 218 kJ/mol for short-term aging of Rene 80, reported by Safari et al in 2006. [42] Although varying, both values for activation energy of coarsening are consistent in that they are lower than the accepted activation energy values for diffusion of both Al and Ti through nickel. [43] This is explained by the fact

that activation energy for a particular reaction may vary with the thermodynamic conditions of the system or parameters of the experiment. [12, 38, 41, 42]

Kinetics of coarsening have been modelled, correlated experimentally, and found to be dependent on factors such as initial precipitate size, initial volume fraction of precipitate, and distribution of precipitate sizes. At an atomic level, progression of long-term coarsening depends mainly on interfacial energy of the particles, but chemical potential (concentration of solute) is also critical, since the process by which coarsening occurs is diffusion. Researchers are not in agreement yet whether rate of coarsening is diffusion or interface reaction controlled, although many models assume diffusion control with reasonable correlation. [41, 44, 38, 20]

### 2.3.2 Coarsening with Strain

Ostwald ripening defines the changes in gamma prime precipitates exposed to increased temperatures for long periods of time. Blades, however, are known to experience conditions of loading, and the result produces a different effect on the second phase precipitates. When gamma prime precipitates are at high temperature in the presence of uni- or multi-axial stress, a resultant strain may be induced. The effect of gamma prime coarsening with strain is sometimes referred to as rafting. The presence of strain in high temperature environments does not guarantee the evolution of gamma prime precipitates from cuboidal to rafted in morphology. A significant length of time is typically required for rafting to occur. As with long-term coarsening, the kinetics of rafting have been studied and modelled at length, and similar theories are utilized in predicting the onset of rafted structures. As well, researchers have studied whether the condition poses any benefit to material structure or whether it is a condition indicative of imminent degradation. Some theorize that due to the coalescence and elongation of

the γ' precipitates, like grain boundaries, they may offer some protection from onset of creep, when oriented perpendicular to the principal load direction. [45, 46, 47]

In 1987, NASA researchers presented their results of a study to observe the evolution of gamma prime particles during engine operation. The experiment was designed to observe the changes in morphology of γ' with respect to varying engine operation segments. The engine test rig was equipped with the ability to monitor blade temperature and stress at root, midspan and tip locations. Following engine testing, subject blades were cross-sectioned at locations representative of leading and trailing edges of the blade and prepared by standard metallographic technique for microstructural evaluation. The objective of the experiment was to establish a potential range of stress and temperature across which gamma prime would transform to its rafted structure. The shortest test segments observed was 27.5 hours, which were long enough to produce rafted structures within blades. Higher temperature and stresses were found to accelerate the rate of rafting in subject blades, and increasing the time at maximum temperature reduced the amount of stress required to initiate rafting. The range of stress and temperature within this study reported to induce rafting of γ' was 15.0 ksi (103.4 MPa) < σ < 19.4 ksi (133.8 MPa) at 1750ºF (954ºC), and approximately 20.2 ksi (139.3 MPa) at 1720 ºF (938ºC). The study is relevant in quantifying conditions of stress and temperature in a typical gas turbine engine, and also illustrates that although a condition observed in material subjected to stress at high temperature, the transformation of second phase γ' from cuboidal to rafted requires a significant length of time. [39]

### 2.3.3 Creep Prediction

Creep is another widely studied phenomenon observed in turbine blades that have been removed from service. It is the term which describes the long term response of material exposed to load and high temperature in terms of material strain. The effects of creep on second phase precipitates do involve diffusion-driven morphological changes such as coarsening and elongation of gamma prime. Since the premise of this study is to observe the response of gamma prime precipitates to high temperature and loading, it would be imprudent not to address creep, which, like precipitate dissolution, is a function of temperature, time and stress. Conditions of creep, if allowed to proceed to the tertiary state, will result in material rupture. Observation of gamma prime precipitates subjected to short-term overtemperature may be thought to exhibit or resemble the physical characteristics of creep-induced changes. However, what research is available describing the effects of short-term overtemperature suggest it is a much less critical condition. Creep is therefore included here for comparison only, and has not been reviewed in detail within this section. [48, 49, 50]

The bulk of studies of turbine blade material have been conducted to represent the "equilibrium" conditions of engine operation, meaning conditions when temperature remains relatively constant within the specified operating range, and the applied load induced by rotation of the engine is within the design limits of the component. Equilibrium engine conditions are useful in representing the predominant conditions experienced over the life of a blade. The evolution of precipitates discussed in the above sections are under these types of "equilibrium" conditions, and all involve time periods of hundreds to thousand(s) of hours. Such conditions have been well-studied and research has contributed to understanding of component behaviour during engine operation and to determinations of component life limits. [18, 20, 28]

Less common, are investigations into non-equilibrium events experienced during engine operation. There are two reasons for this apparent lack of research:

- It makes practical and fiscal sense to prioritize understanding the most frequent or highest likelihood mode(s) of failure, such as corrosion and cracking due to fatigue and/or creep.
- In the absence of data, it is common practice for the aerospace industry to adopt limits conservative enough to yield premature removal of potentially serviceable material, rather than allow continued operation of potentially discrepant material. (ie. Type I vs Type II error) [51]

Short-term overtemperature is one such condition with both a low frequency of occurrence, and an absence of evidence to prove whether an event results in continued good performance or in imminent degradation of the material.

## 2.4 Gas Turbine Engine Operating Conditions

### 2.4.1 Hot Section Environment

The "hot" section of a gas turbine engine is the most severe operating environment within the engine where materials experience a combination of extreme temperatures, high pressure, complex schemes of loading and exposure to corrosive gases. Temperatures in the combustion section can crest 1400ºC (approximately 2500ºF), and even "cooled" components within the turbine section may operate at temperatures close to 850ºC (approximately 1500ºF). Engines are designed to dissipate heat efficiently where possible to prevent long term material degradation, and many components are designed with cooling holes or features whose purpose is diversion of hot gas. Regardless of the ability of a component to dissipate heat, the operating temperatures of

components aft of combustion are still considered “hot” relative to other engine components: hence the term “hot section”. [1, 37, 52]

As introduced in earlier sections, cyclical centrifugal forces are present in the rotating components, and even stationary components may be considered critical for structural reasons, therefore must be capable of retaining strength. Turbine blades in particular experience varying temperature from root to tip, where temperature mid-span has been recorded to be higher than for the root (location mating to the wheel) and tip (location in close clearance to vane-casing wall). [39] With respect to the stress profile, which varies not only from root to tip, but also from leading to trailing edge of the blade, different operating conditions can produce different stress profiles. Mechanical centrifugal and vibrational forces, thermal loading, and gas pressure during operation are all sources of stress which contribute to the overall stress profile for a blade. [53, 54] When combining the conditions of high temperature and demanding loads with the presence of the corrosive products of combustion in the case of gas path components, there is no question why the environment is considered severe. As mainline rotating components within the gas path directly after combustion, first stage turbine blades are subject to strict inspection criteria after service and prior to being deemed “flight-worthy” for return to service. In their published case study on condition assessment of gas turbine blades, Rajendran et al. [55] concluded that microstructural degradation of blade material during service is unavoidable, stressing that operators must adhere to specified limits and recommendations for replacement between overhauls.

In some cases, operation of flight engines beyond recommended limits can lead to premature degradation of critical components. Transport Canada is responsible for regulating civil aviation and issues documents on behalf of engine manufacturers to assist in communicating conditions

of potential abnormal flight risk. [51] Pratt & Whitney Canada issued one such advisory cautioning operators of PW100 engines in "harsh" environments. In the document, a "harsh" environment is specified as, but not limited to environments in presence of sand or dust particulates. Operators were experiencing a higher occurrence of blade distress as a result of blocked cooling holes in blades. Recommendations include continued monitor of in-flight data devices, and increased frequency of scheduled inspection and maintenance. [56] An additional Service Difficulty Advisory titled "Compressor Turbine Blades" targets PT6 engine operators. The advisory urges operators not to run the engine beyond recommended power levels because of its risk to reducing blade life. A higher occurrence of reported premature blade failures due to creep has instigated recurring releases of these Civil Aviation Safety Alerts and recommends increased monitoring for sulfidation, oxidation and blade erosion. The Safety Alert was released in 2007 and continues to be a current advisory. [57]

### 2.4.2 Short-term Over-temperature

The inspection criteria and disposition following a logged occurrence of short-term over-temperature are specified for each engine type by the original equipment manufacturer (OEM). Engine maintenance providers are supplied with proprietary overhaul manuals containing inspection limits and disposition instructions for components that exhibit conditions beyond serviceable limits. Should a component exhibit conditions that exceed repairable limits, the component is typically not returned to service. In the case of one engine model, for turbine blades exposed to short-term overtemperature, the service manual contains a graphical representation showing regions of time and temperature that correspond to blade disposition of a)

acceptable for return to service, b) removal from the engine and visual plus fluorescent penetrant inspection (FPI) performed, c) removal from engine, visual and FPI performed and 2 blades sectioned for microstructural evaluation, or d) all turbine blades removed and scrapped. In the case of this particular engine model, which is not indicated herein to observe proprietary rights, it is acceptable for an engine to reach 790ºC for up to 10 seconds. Exceeding 830ºC for more than 2 seconds requires the visual and FPI inspection, and exceeding a temperature of 850ºC for more than 2 seconds is cause for all compressor and turbine blades to be discarded. [58]

Multiple iterations of blade design, potentially incorporating multiple substrate materials, may be acceptable for operation within a particular engine. The following alloys are all potentially acceptable blade substrate materials in Pratt Whitney engines: B1900, CM 247LC, IN738, IN792, MAR-M-200Hf, MAR-M-247 as well as a handful of PW proprietary nickel-base alloys. [10, 52, 58] From Sponseller's analysis of some well-known superalloys, the practical γ' solvus temperatures for three of the above listed alloys (MAR-M247 = 1246ºC, B1900 = 1224ºC and IN738 = 1182ºC) may be compared as follows:

$$T_{\gamma',solvus}\text{ (MAR-M-247)} > T_{\gamma',solvus}\text{ (B1900)} > T_{\gamma',solvus}\text{ (IN738)} >> 850\ ^{o}C\ [12, 58]$$

Considering the discrete limit of 850ºC for t > 2 seconds has been used to apply to all blade part numbers for the example engine, the factor of safety designed into operation limits is notable.

Dissolution behaviour is important to understand in the application of turbine blades, because the range of engine operating temperatures may at times overlap with the γ' solvus temperature range. The effects of material having been exposed to these temperatures of interest, as well as the conditions leading to peak temperature are important in understanding whether the main strengthening phase of the Ni-base superalloy is capable of retaining its mechanical properties

under duress of the environment. Failure to retain the desired properties of γ' can lead to premature failure of the component. It is therefore prudent to investigate each superalloy under varying ranges of conditions to establish the conditions capable of producing only solid state dissolution versus liquid state dissolution. This is the justification behind the experimental parameters of the current work which looks at the resulting microstructure of DS Rene80, following a series of "short-term" thermo-mechanical regimes.

## 2.5 Scope and Objective of Current Research

Operating specifications for flight derivatives of gas turbine engines generally suggest that exposure to temperatures above specified limits may have a deleterious effect on the mechanical properties of critical components, regardless of the duration of temperature exposure. Removal of an engine having experienced over-temperature from the engine, as well as removal and potentially replacement of turbine blades is a common outcome of this engine condition. Extensive research has been conducted studying the long-term effects of temperature and stress on the micro-structure, and therefore material properties of many superalloys used to produce blades, including the study carried out by NASA, investigating these effects using actual blades within the research.

The current investigation was initiated in order to study the effects of temperature and stress on microstructure of a DS nickel-base superalloy, while limiting duration of exposure to dwell times classified as "short-term".

Key objectives of this experiment are as follows:

1. To simulate multiple scenarios of “short-term over-temperature” in a representative directionally solidified nickel base superalloy by using a Gleeble Thermo-mechanical test apparatus.

2. To document observed changes in the microstructure showing the effects of time (t), temperature (T) and stress (σ), by analyzing samples under Scanning Electron Microscope (SEM), and by using volume fraction of gamma prime precipitates to gamma matrix (γ’:γ) as an indicator and quantification of these effects.

The majority of experimentation was carried out at the University of Manitoba, within laboratories of the Department of Mechanical Engineering. Additional testing was also performed at the University of Waterloo, within the Gleeble laboratory of the Department of Mechanical Engineering and Mechatronics. All metallurgical analysis was conducted in Winnipeg by the author of this thesis.

# Chapter 3

# Experimental Procedure

## 3.1 Material Preparation

The material used for all experimentation is directionally solidified Rene 80, received in plate form and in a partially solutioned state of heat treatment from PCC Airfoils, Inc. Material was received with a chemical certification from Nadcap Materials Testing Laboratory, indicating that the chemical composition of the subject material conformed to the applicable specifications. The nominal composition of Rene 80 has been presented in Table 2.1.

The first sample set for time- and temperature-dependent simulation experiments were water jet machined to size by Metal-Tech Industries Inc. Resulting specimens measured 100 mm in length x 5mm in width x 3mm in thickness. Samples were then heat treated in a vacuum furnace to achieve a uniform state of second phase precipitation, using the following regime: In one hour, heat to 1052 ºC and hold for 4 hours; furnace cool to 843 ºC in 30 minutes and hold for 16 hours; furnace cool to room temperature. This two-stage precipitation heat treatment induces precipitation of the gamma prime phase during the first segment, and the longer time at a lower temperature represents the aging segment during which second phase precipitates have time to achieve moderately uniform size, resulting in a reasonably homogenous state of precipitate within the gamma matrix. Following heat treatment, samples were prepared for Gleeble simulation by manually removing surface oxides, then spotwelding thermocouple wire at three locations along the length of each specimen. The thermocouples allow for monitor of sample

temperature and feedback to the Gleeble program during simulation testing. Samples were sectioned at each of the thermo-couple positions following simulation using a Hansvedt DS-2 Model wire Electro-Discharge Machine. Cutting at the location of the spotweld serves two purposes: a) the spotweld provides for a unique feature easily identifiable at high magnifications, and b) the area immediately adjacent to the spotweld contains microstructure most accurately representative of the reported temperature.

Sectioned specimens were then mounted, ground and polished using standard metallographic techniques. In order to reveal the gamma-prime phase (γ'-phase) for micrographic analysis, samples were electrolytically etched with a "Gamma-prime" etchant at 3 Volts for 4 to 6 seconds. The gamma prime etchant is a solution of 144mL $H_2SO_4$ + 120mL $HNO_3$ + 36 mL $H_3PO_4$. Etched samples were then analyzed by Scanning Electron Microscope, the details of which are presented in the next sections.

For the second phase of testing, additional samples of DS Rene 80 stock were machined on the Hansvedt EDM in accordance with the configuration depicted in ASTM E8M, "Rectangular Tension Test Specimen," for conducting Gleeble samples with an applied tensile load. Specimens exhibited an overall exterior dimension of 100 mm long x 25 mm wide, and were drilled with 6mm diameter holes in order to accommodate the Gleeble grip assembly. [59] Figure 3.1 contains a photograph of a representative sample. After machining, the tensile test specimens were processed through the vacuum furnace using the same heat treatment described above in order to achieve a consistent microstructure prior to testing. Following thermo-mechanical simulation, samples were prepared in the same manner as the time- and temperature-dependent test samples including cross-section using the EDM, mount and preparation using

standard techniques and following the same procedure for etching with the Gamma prime solution.

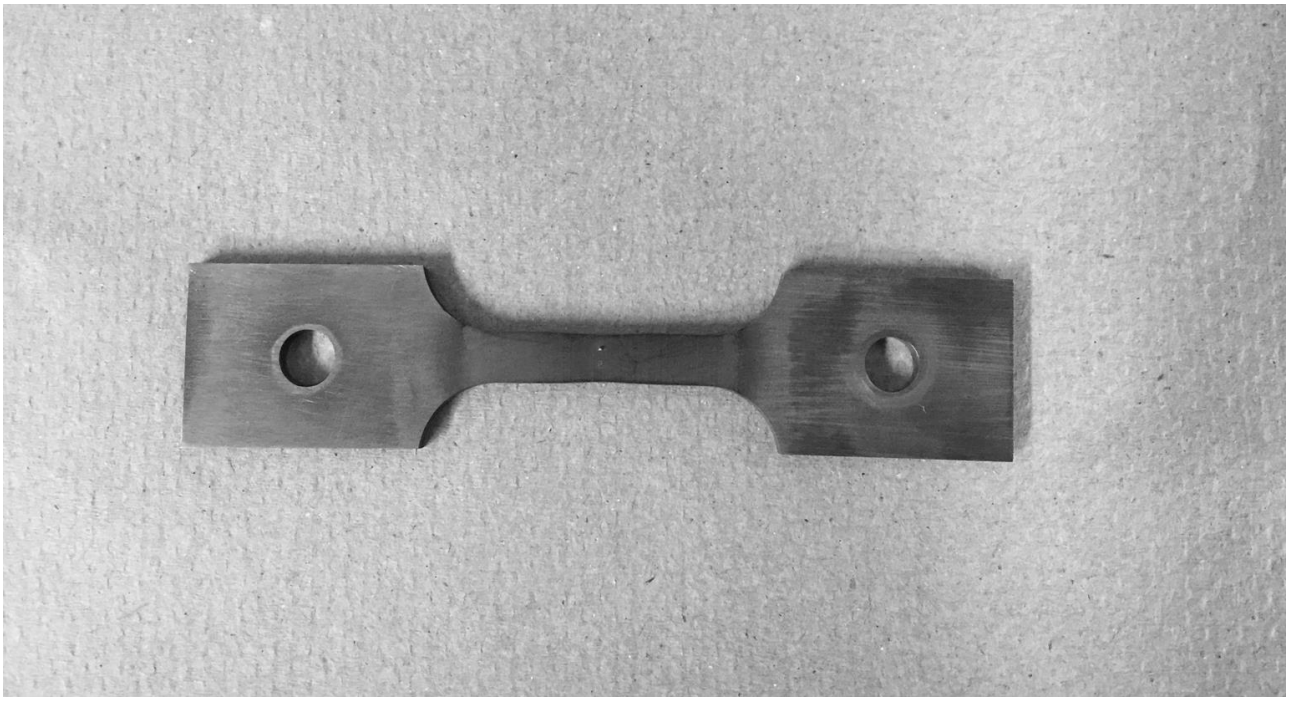

**Figure 3.1: Gleeble test specimen machined to configuration and dimensions specified within ASTM E8 [59]**

## 3.2 Gleeble Thermal and Thermo-mechanical Simulations

Experiments to create varying microstructures to observe the effects of time and temperature on dissolution of gamma prime were carried out using a Gleeble Thermomechanical Simulator. The Gleeble apparatus responds to a computer controller which may be programmed to subject test specimens to high temperatures using specified parameters of time to target-temperature (heating rate), time at target-temperature (duration), and engagement of a tensile or compressive load. The first phase of experimentation for this thesis included only thermal simulation, exposing samples to varying temperatures between 1130 ºC - 1190 ºC for a constant time of 1 second. All samples in the first phase were run using a distance of 30 mm between the water-cooled copper jaws. The heating rate used for all Gleeble simulations was 36.9 ºC/second. This heating rate was calculated to represent typical engine start-up conditions (time to reach specified operating temperature), which is an example of a scenario during which over-temperature may be observed in aircraft engines. [52, 58] A schematic of a typical thermal profile from the initial phase of testing is shown within Figure 3.2. It can be seen in the thermal profile graphic that quenching was utilised as a mechanism for cooling from the target temperature. Water-quenching after holding at target temperature for 1 second (for all temperature-dependent testing) was performed to ensure the microstructure of each sample would be representative of the condition resulting from heat and time inputs to the material. Time-dependent thermal simulations were conducted under isothermal conditions at 1150 ºC for varying times ranging from 1 - 20 seconds to observe the changes to morphology of γ’ and volume fraction of γ’:γ over a series of “short-range” times. The same heating rate and jaw distance were observed during this series of testing. Table 3.1 showing Gleeble test conditions is included for reference.

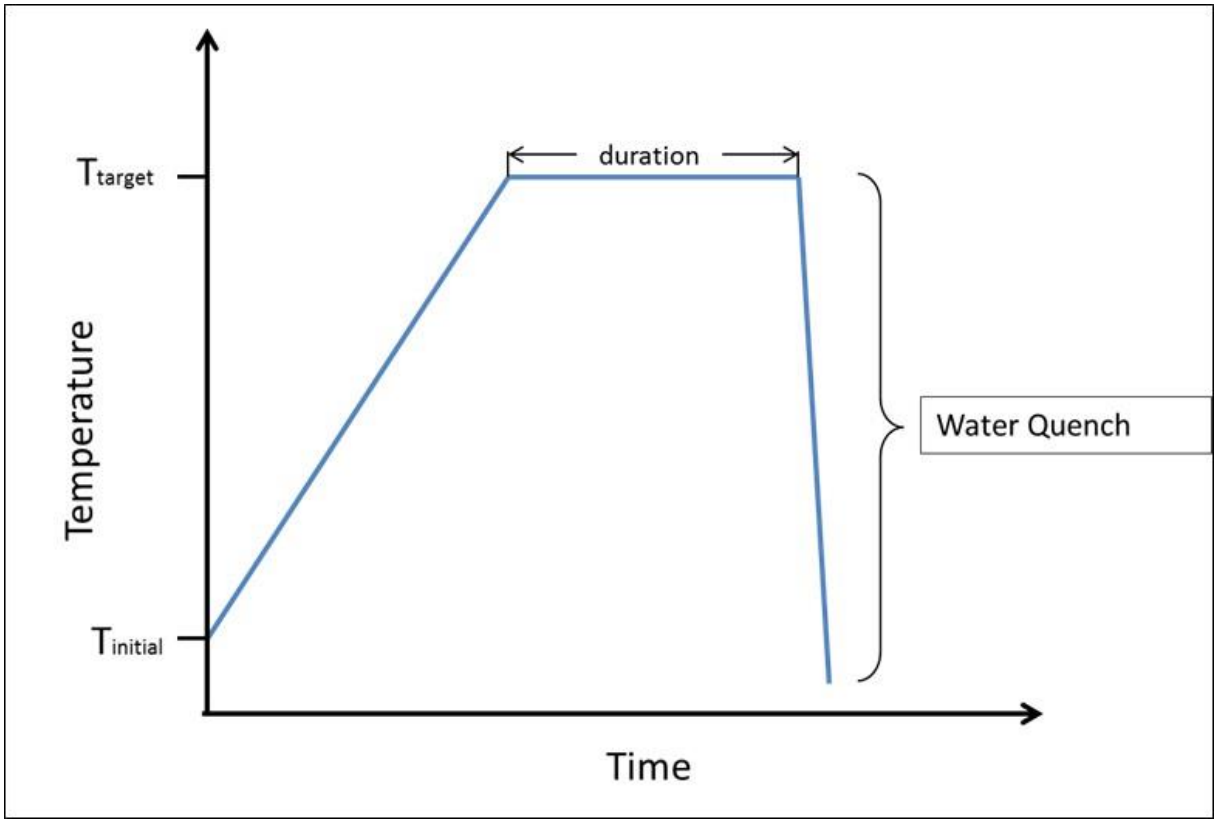


**Figure 3.2 Schematic representation of a typical heating profile produced by Gleeble program.**

A second phase of testing was conducted in order to observe the effects of stress. The parameters of time and temperature were held constant at t = 2 seconds and T = 1150ºC, while applying varying tensile loads on test specimens. The test values for load were acquired by first subjecting a sacrificial sample to a programmed stroke length of 10.0 mm. The resulting force measured at the point of rupture, $F_R$, was then used as an upper limit, and test values of $F_R/4$, $F_R/3$ and $F_R/2$ were assigned. For all simulation testing involving load, the same heating rate of 36.9ºC/second was used. It should also be noted that the Gleeble was programmed to apply the tensile load at test initiation and then commence heating to the target temperature of 1150 ºC. For all tests, quench was initiated after a dwell time of t = 2 seconds at peak temperature and under target load.

Due to an unrecoverable hardware failure within the computer control system of the Gleeble apparatus in the University of Manitoba Materials Laboratory, an additional series of testing was performed at the University of Waterloo, in the Mechanics and Mechatronics Laboratory. The Gleeble apparatus housed at Waterloo was the same make and model as that in Winnipeg. Waterloo load tests were conducted using the same methodology to acquire values for target loading. The initial test began with applying a stroke of 10.0 mm at a test temperature of 1150 ºC, and the force to rupture, $F_R$, was observed. Subsequent load values were assigned based on an observation of "yielding" in the force-to-distance plot, which coincided with a value approximately equal to $F_R/3$. Again, the same heating rate of 36.9 ºC was incorporated within all Gleeble programs. Due to a different configuration of quenching apparatus, samples were quenched manually. Quenching for Waterloo tests occurred after a dwell time of t = 1 second at target temperature of 1150 ºC and test load. The test parameters for this second phase of load

testing are listed within Table 3.1, and the corresponding values of stress for each target load data point have been included as well. It should be noted that cross-sectional area was measured for each individual sample and recorded values for load were used in calculating the corresponding stress values. All stress values have been presented in the unit of megapascals (MPa).

**Table 3.1 - Gleeble thermal and thermo-mechanical test parameters**

| | | |
|---|---|---|
| **Thermal Test Parameters** | | |
| | Heating Rate | 36.9ºC/second |
| | Cooling Rate | Water quench |
| | Jaw Spacing | 30 mm |
| | Target-Temperature Test Values | 1130ºC, 1140ºC, 1150ºC, 1160ºC, 1180ºC, 1190ºC |
| | Time (Duration ) Test Values | 1 , 2 , 10 , 20 seconds |
| **Thermo-Mechanical Test Parameters** | | |
| | Heating Rate | 36.9ºC/second |
| | Cooling Rate | Water quench |
| | Peak Temperatures | 1150ºC, 1050ºC |
| | Duration | 1 second, 2 seconds |
| | Target Tensile Load Values (Corresponding Stress Values) | |
| (Winnipeg Gleeble) | 0 kN (0 MPa), 0.9kN (49.4 MPa), 1.2kN (65.8 MPa), 1.8kN (98.8 MPa) | |
| (Waterloo Gleeble) | 0 kN (0 MPa), 0.6 kN (33.2 MPa), 0.8kN (42.7 MPa), 1.0kN (55.6 MPa), 3.1 kN (161.7 MPa) | |

## 3.3 Microscopy

Microstructures of all samples were examined using a Zeiss optical microscope to a maximum magnification of X1000. To observe samples at higher magnification, scanning electron microscope (SEM) was utilized. For a subset of the initial test samples involving only varied conditions of time and temperature, but with zero load, micrographs were obtained using a Philips XL30 SEM, and then analyzed using CLEMEX Vision 3.0 image software to obtain digitally computed values for volume fraction of γ':γ . In addition to the Clemex software, a standardized manual point count method (ASTM-E-562, Determining Volume Fraction by Systematic Manual Point Count) [60] was also used to quantify volume fraction. Both methods for obtaining quantitative volume fraction data were used when possible. At times, due to limitations of the CLEMEX software, only the manual point count method was used. Additional analysis was performed using a JEOL 5900 SEM in the secondary electron emission (SE) mode. Due to variations in the volume fraction of gamma prime in some samples, etching conditions were modified such that sufficient contrast could be obtained in the sample surface for adequate analysis under SEM. Because the etching solution is meant to reveal the γ' constituent, longer etching time or higher voltage was required in some samples with lower overall fraction of γ' phase (greater degree of dissolution). There is also variation from sample to sample in the working distance in order to achieve the best possible resolution for each sample during scanning. This variation results in micrographs being obtained at a variety of magnifications, but allows for appropriate relative comparison between sample conditions. The analysis results are presented in the following chapter and discussion of relevant theories is also presented.

# Chapter 4

# Results and Discussion

## 4.0 Introduction

The results of the investigation of short-term overtemperature of directionally solidified Rene 80 are presented within this chapter. Analyses of microstructural changes occurring due to temperature, dwell time at peak temperature and addition of an applied tensile load are included. The discussion sections contain theories to explain the observed changes in microstructure and the atomic mechanisms required to yield these changes. Some observations regarding the kinetics of dissolution are included, and the chapter concludes with comments regarding limitations of the current research.

## 4.1 Microstructural Analysis of Test Specimens

This section contains micrographical representations of the different conditions of experimentation, observations regarding the microstructural changes produced, and quantification of the observed volume fraction of precipitate to matrix for the various conditions. Study of the material specimens begins with a review of an "untested" sample, which has undergone the standard precipitation heat treatment (PHT), but has not been exposed to any subsequent Gleeble testing. The section then continues with presentation of data and observations regarding the Gleeble specimens.

### 4.1.1 Precipitation Heat-Treated (PHT) Microstructure

Study of the precipitation heat treated (PHT) sample is important because it is representative of the material condition of components prior to service. Understanding the microstructure of the material before exposure to any short-term overtemperature is necessary to assess what changes are occurring as a result of the variations in temperature and dwell time at peak temperature. Figure 4.1 contains SEM micrographs of the PHT sample. Carbides are evenly dispersed throughout the alloy and can be seen at the lower magnification in Figure 4.1 a), present in blocky and script morphology. Energy Dispersive Spectroscopy (EDS) scan of an MC carbide (Figure 4.1 b) revealed the carbide to be rich in Ti, W and Mo. The presence of block-type MC carbides rich in Ti, W and Mo for Rene 80 in its PHT state is consistent with published data. [14]

The heat treatment performed includes stabilization at a temperature of 1052 ºC (4 hours) and aging at 843 ºC (16 hours), which produces relatively homogeneous distribution of second phase γ', which appear uniform in size. Upon closer examination, it can be observed that the cuboidal γ' particles actually vary in edge length. The inset in Figure 4.2 illustrates the size difference between edge length of γ' particles from approximately 0.25 µm to 0.6 µm. In the PHT sample, the average precipitate size was calculated to be 0.5 µm. Quantification of the fraction of area of γ': γ across a series of sample sites yielded an average of 69%, which is also consistent with the observations of other researchers for microstructure of precipitation heat-treated Rene 80. [14, 20, 42, 61] Volume fraction data for this sample were acquired using the Clemex Vision software, as well as calculated using the manual point count method. [60, 62] Values were found to correlate well between the two methods. Although micrographs used are representative of area fraction, due to the cuboidal nature of the γ' precipitates, area- and volume-fraction are used as interchangeable expressions within the current research. [63]

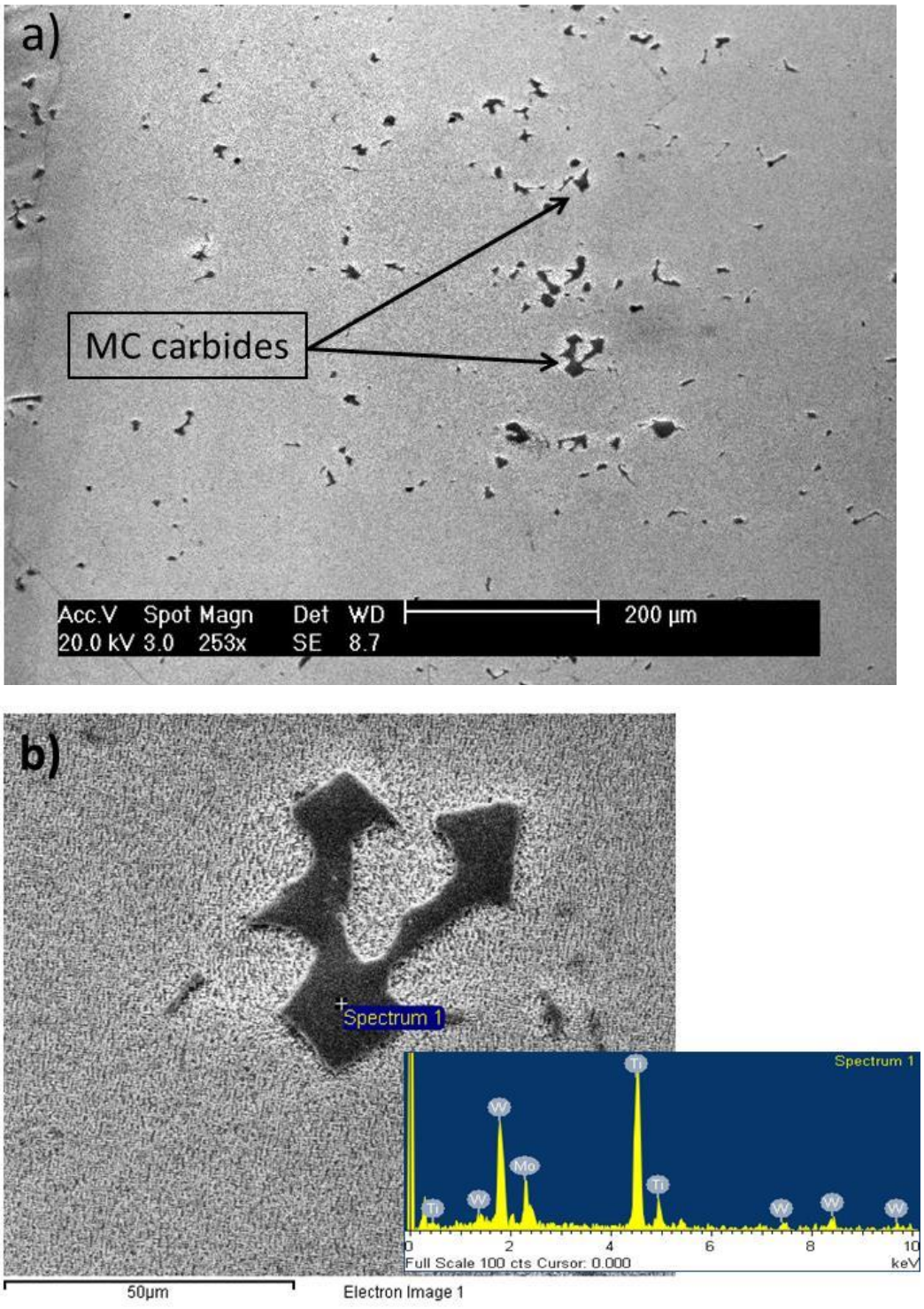


**Figure 4.1 a) SEM micrograph showing distribution of block- and script-type MC carbides and b) EDS scan of a representative carbide rich in Ti, W and Mo**

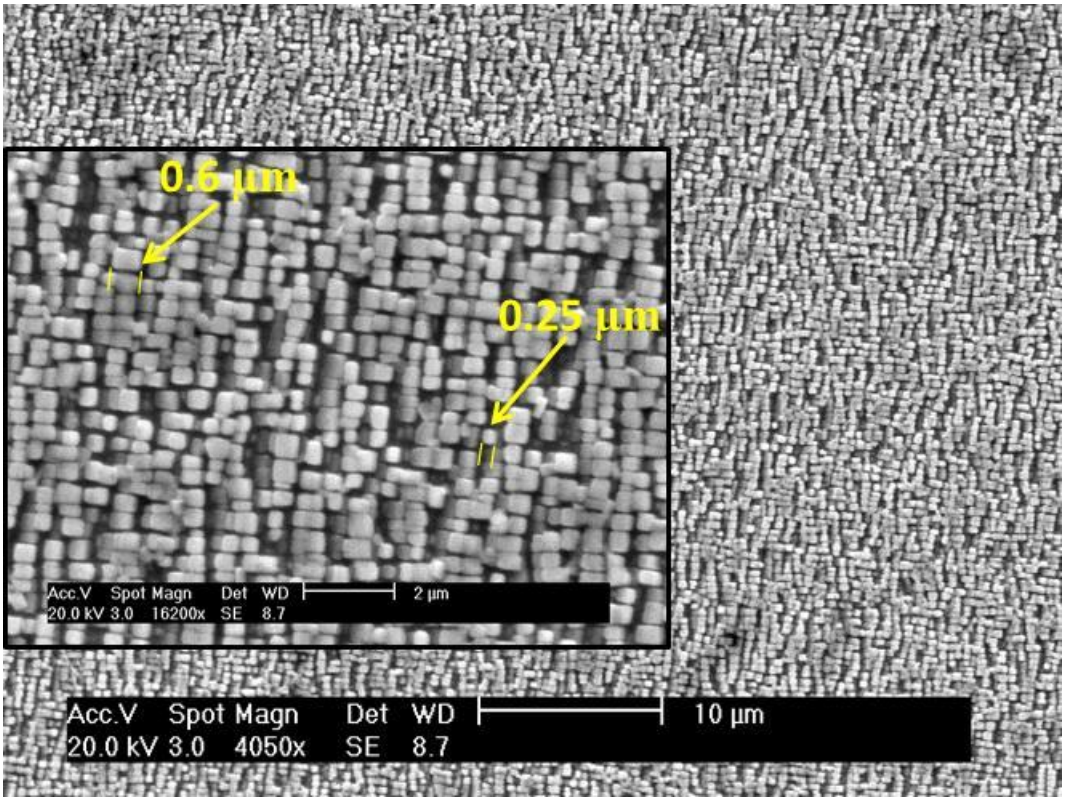


**Figure 4.2 SEM micrograph of the PHT sample illustrating the difference in edge length of γ' precipitates**

### 4.1.2 Gleeble Samples

Three series of Gleeble study were performed in an attempt to isolate the effects of temperature, of time and of stress on the dissolution behaviour of the γ` strengthening phase. The results of each study are presented in the following sections.

#### 4.1.2.1 Variable Temperature Testing

Initial Gleeble experimentation was conducted using the heating rate of 36.9 ºC/s to a series of peak temperatures ranging from 1130 ºC to 1190 ºC and holding for a constant dwell time of 1 second. Peak temperatures were chosen as temperatures of interest, based on the reported "practical" dissolution temperature of T = 1150 ºC for Rene 80. [4] Figure 4.3 contains a series of SEM micrographs representing the various samples. Visual comparison of the different samples illustrates a significant decrease in volume fraction with increasing peak temperature. For the lowest peak temperature of 1130 ºC, some evidence of γ' dissolution is present, and complete dissolution has not occurred at the highest peak temperature of T = 1190 ºC. The greatest change in volume fraction occurred between peak temperature set points of 1130 ºC and 1140 ºC, a reduction of approximately 50% in fraction of γ':γ.

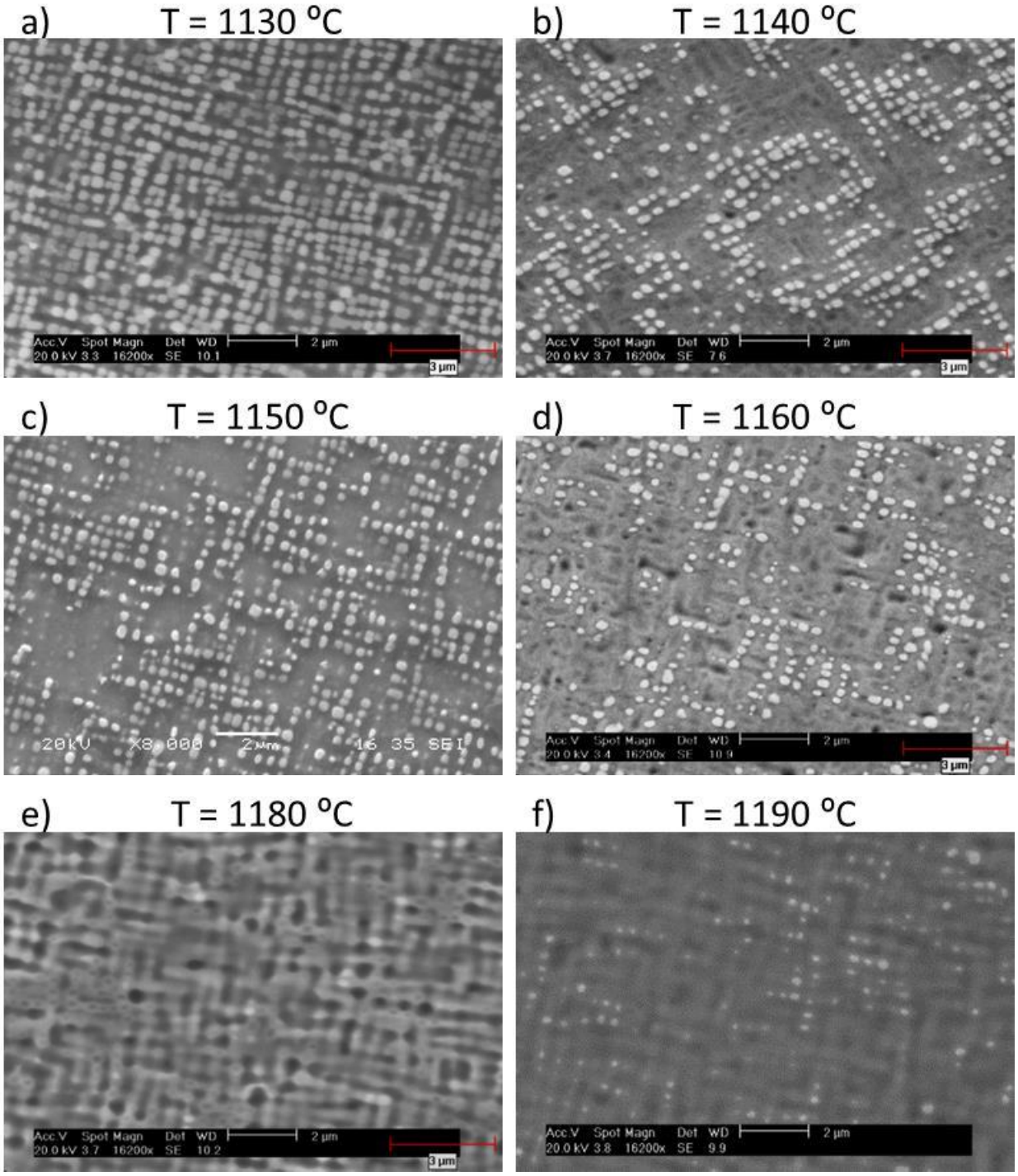


**Figure 4.3** SEM secondary electron images of the variable temperature samples showing significant reduction in volume fraction with increasing temperature and 1 second dwell.

The temperature range of test points in this study is 60 ºC. Other research shows it is common for a second phase dissolution transformation (like γ' precipitates) to occur across such a temperature range, and for that range to increase in value with increasing heating rate. [20, 64] In their study by differential thermal analysis (DTA) of IN713LC, Zla et al., observed the largest temperature interval between initiation and completion of γ' dissolution to coincide with the fastest applied heating rate. They also found heating rate to cause a shift in the onset and completion temperatures of particle dissolution where faster heating rate yielded a higher temperature. [65]

As well, the morphology of the γ' precipitates progresses from nearly cubic in its PHT state (Figure 4.4 a), to cuboidal in the 1140 ºC and 1150 ºC samples (Fig. 4.3 b and c respectively), to rounded at the highest peak temperature sample (Figure 4.3 f). Sizes of the γ' precipitates reduce with increasing temperature. At the highest test temperature of 1190 ºC, there are very few particles remaining undissolved and they have reduced in size to an average diameter of 0.18 µm, with a maximum diameter of particle measuring 0.25 µm. Graphical representation of the calculated volume fractions of γ':γ for each variable temperature sample and their corresponding average particle size is presented in Figure 4.5 a).

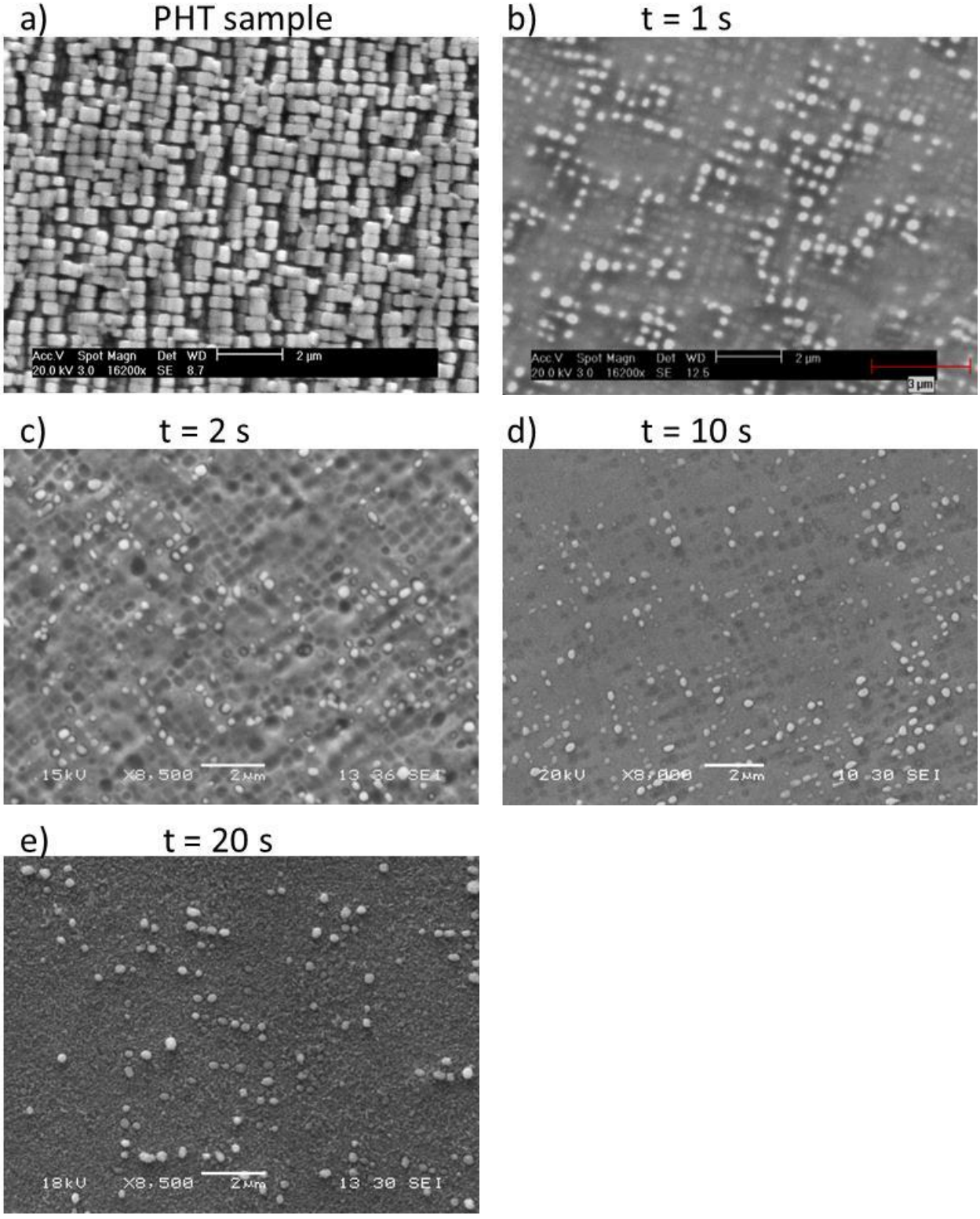


**Figure 4.4 SEM secondary electron images showing changes in volume fraction, size and morphology of γ' with increasing dwell time at T = 1150 ºC**

### 4.1.2.2 Variable Time Testing

For the variable time experiments, the heating rate of 36.9 ºC/s was again used to achieve a constant peak temperature of 1150 ºC for varying dwell times. Figure 4.4 shows SEM micrographs representing isothermal testing for the variable times. As with the variable temperature test data, the decreasing volume fraction is accompanied by an evolution in the γ' precipitate morphology from cuboidal to rounded, and the average size of precipitate reduces from approximately 0.5 µm for the 1 second dwell time (Figure 4.4 b) to 0.2 µm after a 20 second dwell time (Figure 4.4 e).

Again, for each sample, volume fraction quantification was performed on multiple sites and an average taken to represent the particular test condition. Volume fraction reduces with increasing dwell times, easily seen in Figure 4.4, with the bulk of dissolution occurring in the first second of dwell time. For dwell time of 1 second, the calculated volume fraction is 19% γ':γ. Considering the initial PHT volume fraction value of 69%, this test yields a reduction in volume fraction of approximately 72%, which is a significant amount of dissolution occurring in the first second at the peak temperature. Giraud et al observed the greatest decrease in γ':γ to occur in the first minute of dwell time and refer to the behaviour as the "first transient stage" of dissolution. [66]

Given that the target temperature coincides with the accepted value for an equilibrium γ' solvus temperature (1150 ºC), it is not surprising that a significant amount of dissolution occurs with a very short dwell time at this critical temperature. Researchers of dissolution kinetics have commented that an asymptote in the volume fraction value is indicative of the material approaching thermodynamic equilibrium. [67] This was believed to be tied to the apparent activation energy, Q, being lower at the beginning of the dissolution reaction for a specific

temperature. They reported the following values of activation energy for diffusion in a single crystal alloy at 1100 ºC: 179 kJ/mol for a dwell time of 0 seconds, 187 kJ/mol for a 15 minute dwell and 196 kJ/mol for a 30 minute dwell. (The value corresponding to "zero" dwell time was an extrapolated calculation.) The increase in activation energy with dwell time is explained by the greater instability of γ' particles at the onset of a rapid thermal exposure, and hence less energy being required to initiate the dissolution phase transformation. As the material becomes more stable with a longer dwell time at a particular temperature, diffusion is slower to proceed and requires greater energy to initiate. [67] For the current research, the difference in observed γ'−γ volume fraction between a dwell time of 10 seconds and 20 seconds is 1%. This is not a significant change and may be an indication that the "transient" stage of dissolution is subsiding and thermodynamic equilibrium is imminent.

It should also be noted that for the 20 second dwell time sample (Figure 4.4 e), fine, spheroidal secondary γ' particles may be observed. This is due to a small delay in activation of the Gleeble apparatus water quench solenoid during testing. Secondary γ' were not considered in quantification calculations for volume fraction of that sample. Graphical representation of volume fraction and size with variable time are shown in Figure 4.5.b.

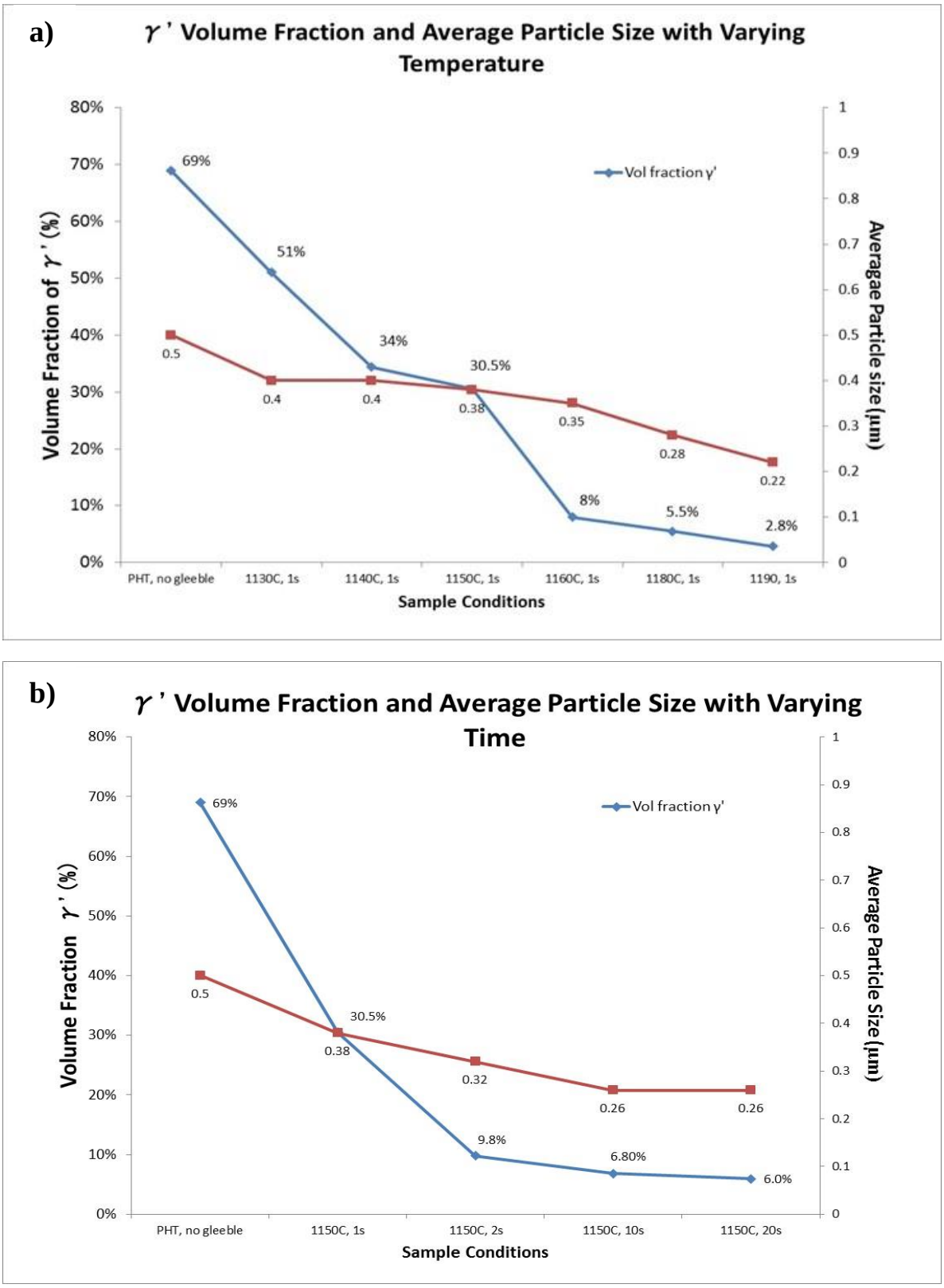


**Figure 4.5 Graphical representations of average particle size and volume fraction with a) variable temperature and b) time**

#### 4.1.2.3 Tensile Load Testing

Once volume fractions had been calculated for the variable time and variable temperature experiments, the parameters were chosen for time and temperature under a tensile load. The load tests were conducted using a constant peak temperature of 1150 ºC and a dwell time of either 1 or 2 seconds. For the testing completed in Waterloo, because quenching of the samples was performed manually, dwell time at peak temperature was not programmed into the Gleeble. Dwell time for these tests was estimated to be 1 second, as opposed to tests performed in Winnipeg where quenching was programmed to occur following a 2 second dwell time at the target temperature. As stated earlier, preliminary testing was conducted to determine the load required to rupture a sample at peak temperature, and fractional values of that load were used as test parameters. Corresponding stress values were calculated later using the measured cross-sectional area for each sample and measured force recorded during Gleeble testing. The stress values are presented within Figures 4.6 and 4.8 along with SEM images of the samples.

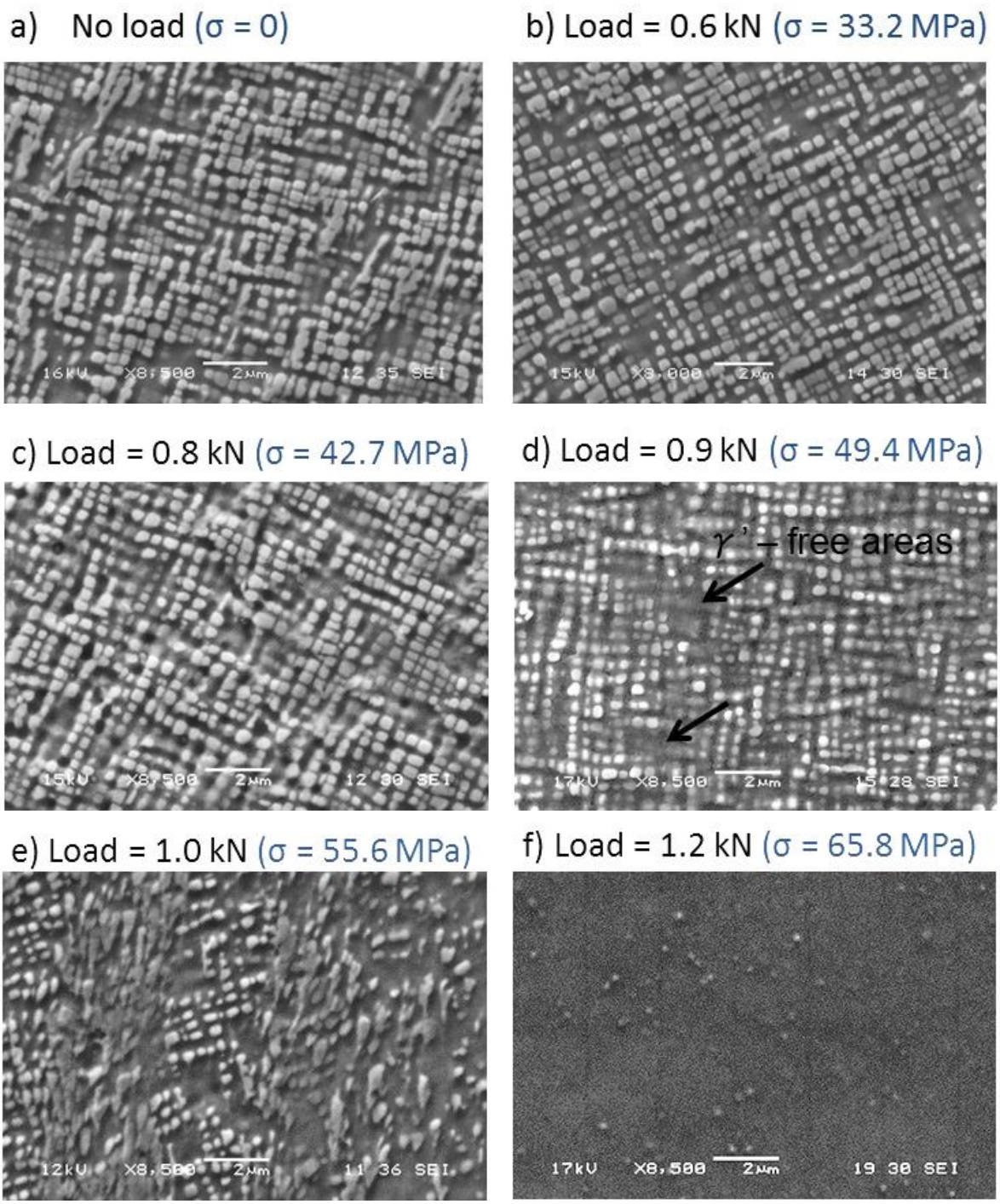


**Figure 4.6 SEM secondary electron images of samples exposed to T = 1150 ºC for 1 second under increasing values of tensile load (corresponding calculated stress value).**

Figure 4.6 compares an unloaded sample to samples exposed to loads of 0.6 kN, 0.8 kN, 0.9 kN, 1.0 kN and 1.2 kN, after reaching a peak temperature of T = 1150 ºC. The images, obtained from two series of experiments, are presented in order of increasing load (stress in parentheses) and show an overall decrease in volume fraction of γ' precipitates. For example, when comparing Figure 4.6 a) the unloaded sample to d) a sample exposed to a 0.9 kN tensile load, which yields a corresponding stress of 49.4 MPa, larger regions of dissolved precipitate may be observed. The inhomogeneous nature of the dissolution of the γ' particles is also notable from these images. The arrows in Figure 4.6.d) highlight a pair of γ'-free regions, which are not uniformly sized or dispersed. This observation is consistent with other researchers' findings that dissolution does not occur homogeneously. [66, 67] The γ'-free areas are small regions where clusters of a few individual γ' particles have completely dissolved. The occurrence of rapid dissolution in certain small clusters of γ' particles is thought to be triggered by elastic interactions between precipitates. [66]

A second series of loaded Gleeble tests were conducted at a lower peak temperature of 1050 ºC ($T_2$) with the objective of further isolating the effect of stress from the effect of temperature. It was hypothesized that at the lower peak temperature, the effects of dissolution due to temperature would be less pronounced and therefore any potential effect due to stress would be more apparent. At the lower peak temperature, $T_2$, a substantially higher force of 9.33 kN was measured at the point of sample rupture than for the testing conducted at $T_1$ = 1150 ºC (where force to rupture $F_{R\ (T1)}$ = 3.02 kN). The corresponding stress values at the measured rupture forces for $T_1$ and $T_2$ are 167.8 MPa and 518.3MPa respectively. As a comparison, the reported ultimate tensile strength of Rene 80 at room temperature is approximately 1000 MPa, (varying between 940 and 1040 MPa depending on the aging treatment). [61] This illustrates the strong

effect of temperature on material strength. Given that $F_{R\ (T2)}$ = 9.33 kN, subsequent target load values for $T_2$ were selected to yield comparison of like force at different test temperatures, as well as one test point selected based on observations of slope change (representative of yielding) in the force-distance plot produced during the test to rupture. The force-distance plot for the Waterloo rupture tests is presented in Figure 4.7 for reference. In each case, an initial yield may be observed just below 1 kN. Given that yielding had begun, strain was thought to be present in the sample at forces greater than 1 kN. The effects of strain, and its potential to modify dissolution kinetics are discussed in section 4.2.3. For both test temperatures a second yield point may be noted just prior to peak force, after which rupture occurs.

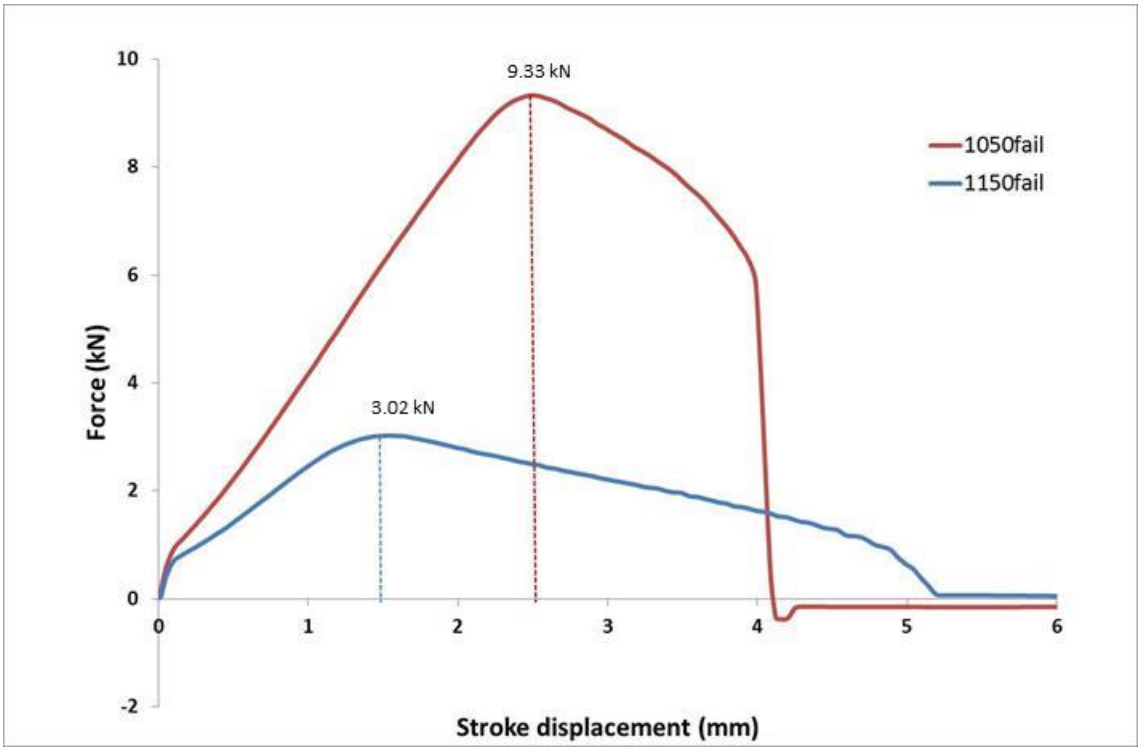


**Figure 4.7: Graphical representation of the tensile tests pulled to failure showing force versus distance for the two test temperatures. Forces acquired were used to establish parameters for the load-dependent test series**

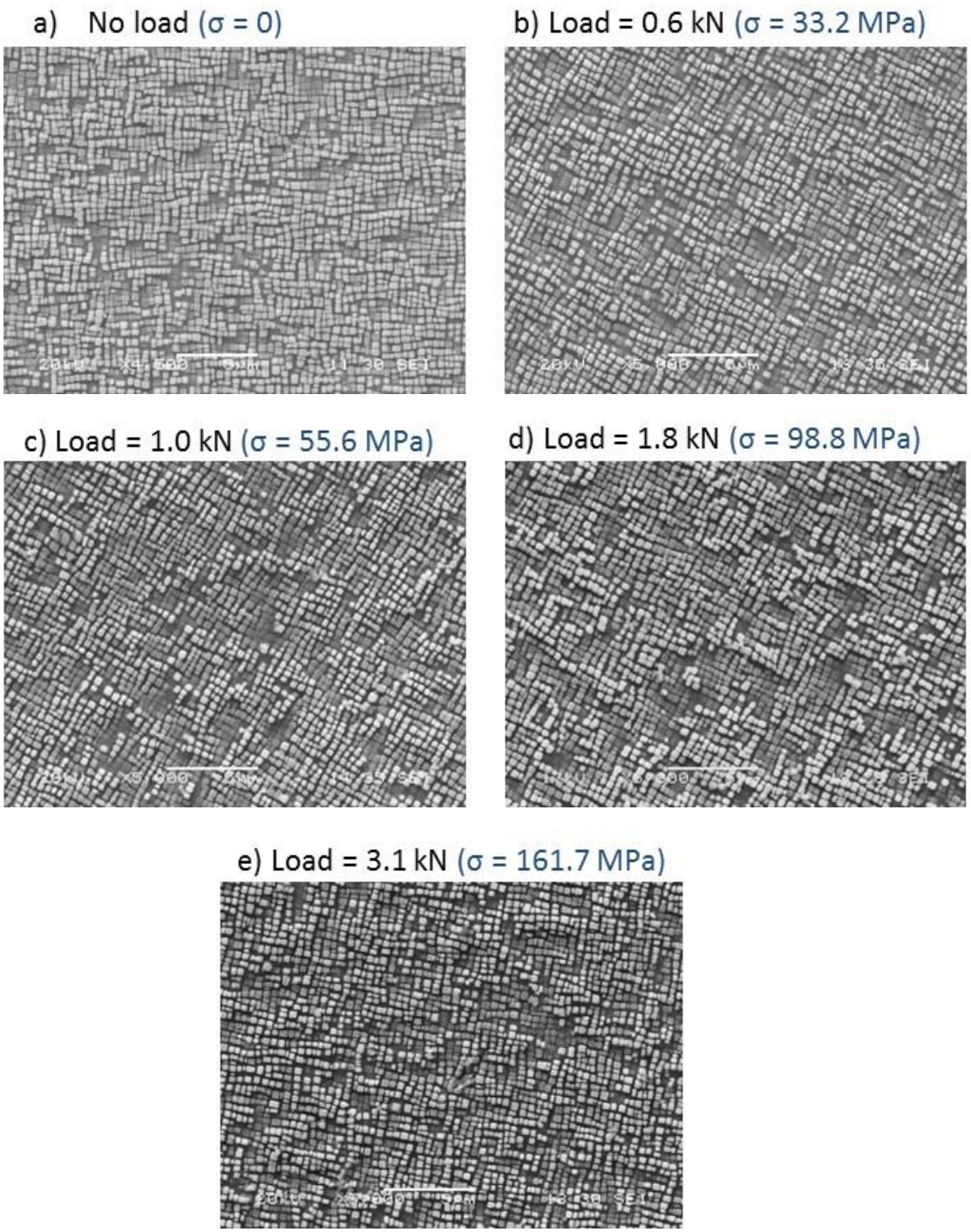


**Figure 4.8: SEM secondary electron images of samples exposed to T = 1050 ºC for 1 second under increasing values of tensile load (corresponding calculated stress value). Scale is 5 µm for images (a) through (e).**

Figure 4.8 contains secondary electron SEM images of the resulting samples, where the changes in γ':γ volume fraction are visually less apparent than for the tensile tests at $T_1$. Quantitative analysis of the images, however, did reveal a reduction in the presence of γ'. For the series of load testing conducted at the lower peak temperature of 1050 ºC, volume fraction of γ':γ decreased from value of 53.3% under no load, to a value of 41.6% under a load of $F_{R\,(T2)}/3$ = 3.1 kN, which corresponds to a stress value of 161.7 MPa. This differential of 11.7 percentage points between the two conditions is greater than the deviation for the individual samples and therefore shows that the applied stress influences dissolution behaviour of γ'. Further explanation of this phenomenon is included in the following section. The graphical results for volume fraction analysis of load testing at both test temperatures are presented in Figure 4.9. For the condition of maximum stress at the $T_2$, the average precipitate size, 0.42 µm, was found to coincide with measurements for average precipitates contained within the unloaded sample for T = 1050 ºC. In both samples, the second phase γ' particles ranged in size from 0.3 – 0.6 µm. Only a reduction in the ratio of γ':γ was observed; no changes in morphology or size of individual γ' particles were noted.

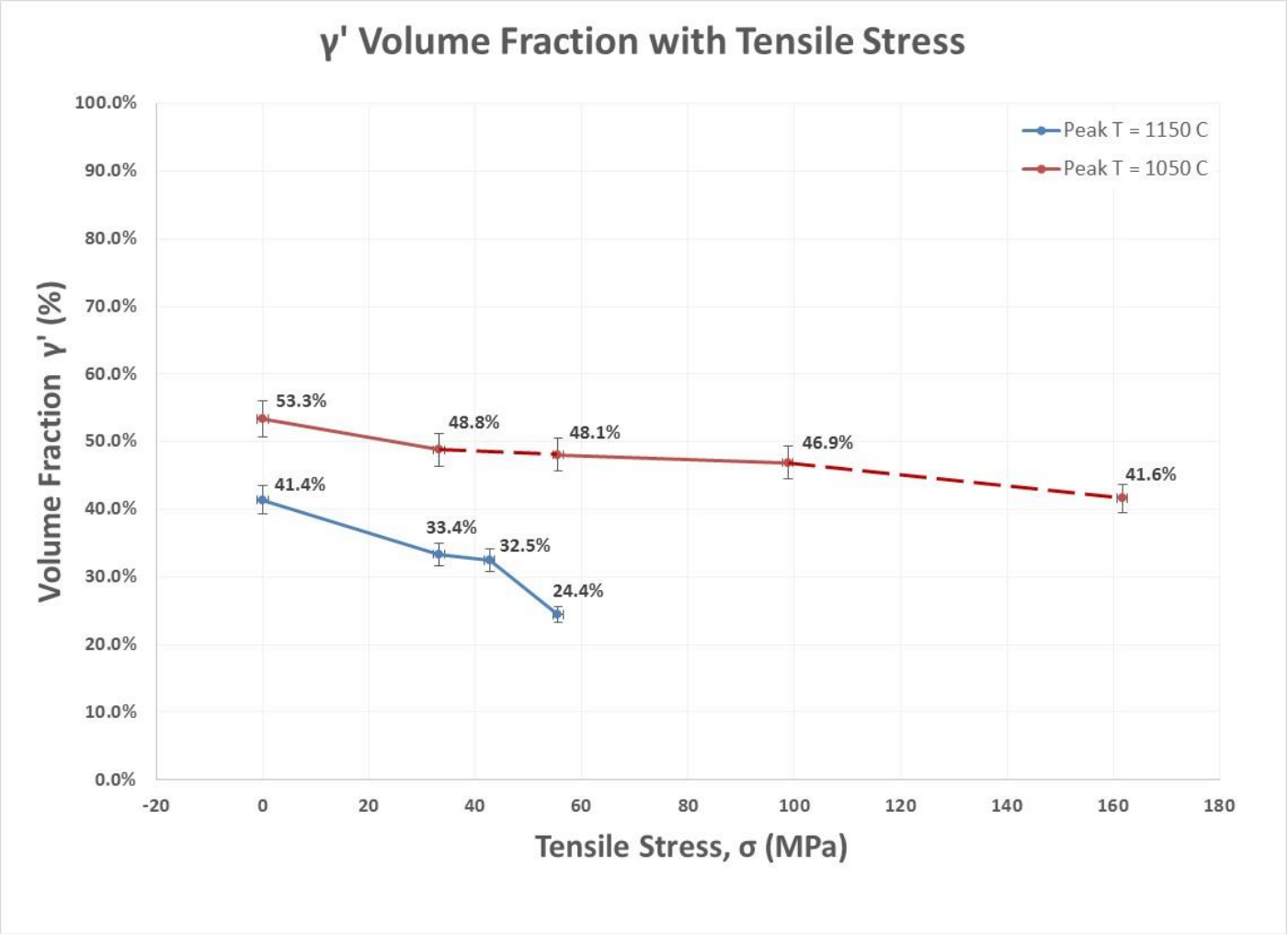


**Figure 4.9: Graphical representation of changing volume fraction with increasing tensile stress for testing to peak temperatures of T = 1050 ºC and T = 1150 ºC**

## 4.2 Progression of γ' Precipitates

In each of the studies conducted, an evolution of γ' particles was observed. Time and temperature testing produced changes to the characteristics of individual particles (size and morphology), and to the resulting volume fraction of γ':γ. The load testing showed an influence of stress on volume fraction of γ':γ . The nature of these changes observed in γ' particles is discussed in the next sections, paying particular attention to which conditions yielded solid state dissolution versus liquid state dissolution, and how the presence of stress appears to have altered the dissolution behaviour.

### 4.2.1 Solid State Dissolution

Per the literature, as previously stated within Chapter 2, solid state dissolution is typically associated with conditions considered to represent equilibrium, where there is sufficient time for material to achieve thermodynamic stability as the temperature is changing. [1, 18] Solid state dissolution of the precipitate phase will occur as the increase in temperature reduces stability of the phase. For Rene 80, in the temperature range approaching the solvus for γ' precipitates, the initial stages of solid state dissolution are accompanied by morphological changes in individual particles. The instability results in corner dissolution [68], which is the first change observed. Particles that may have appeared to be close to cubic in shape become cuboidal shape, and evolve toward rounded or spheroidal shape as they are also reducing in size. Figure 4.10 shows this evolution schematically and using cropped images from the experimental work. The scale for each image has also been cropped and included for perspective of particle sizes.

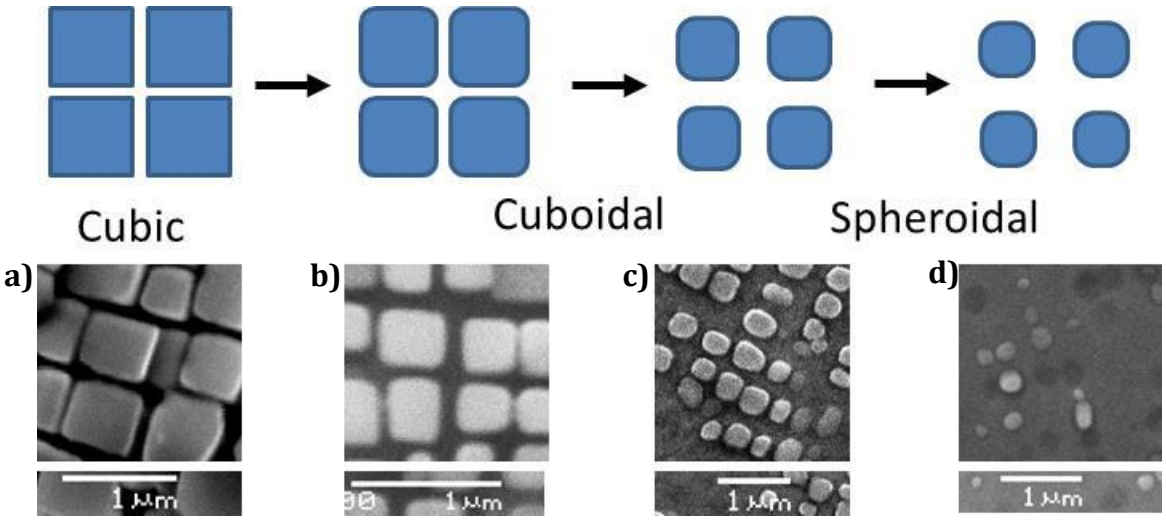


**Figure 4.10: Schematic diagram showing morphological progression of γ' precipitates during solid state dissolution in selected scanning electron images a) PHT b) T = 1050 °C, t = 1s, σ = 0 MPa, c) T = 1140 °C, t = 1s, d) T = 1150 °C, t = 10s.**

Although transition of particles from cubic to spheroidal was observed throughout experimentation, no attempt was made to correlate dependence of the evolution to time or to temperature. The images shown in Figure 4.10 are cropped from samples for the temperature- and time- and stress-dependent studies and are included only to illustrate the observation of morphological changes in precipitates as dissolution proceeds. The observed changes in shape are consistent with other experimental observations [69] and literature describing γ' dissolution behaviour for other Ni-based superalloys. [68, 70]

In their experimental study of the dissolution behaviour of γ' precipitates, Wang et al observed precipitates of cubical, cuboidal and spherical morphology and assert that competition between the interfacial energy and elastic energy components is what determines precipitate morphology. [70] Their position is derived from the work of other researchers who were able to conclude that during precipitate growth, interfacial energy promotes isotropic precipitate shape (eg. spherical) and elastic strain energy promotes anisotropic precipitate shape (eg. cubic-type). The change

observed from cuboidal to spheroidal in the current work may therefore be due to initial dominance of the elastic strain component, which is proportional to precipitate volume, shifting to a dominance of the interfacial energy component, which is proportional to surface area. [71, 72]

For all of the time-dependent testing conducted at T = 1150 ºC (refer to Figure 4.4), and for the temperature-dependent samples tested within the following peak temperature range: 1130 ºC ≤ T ≤ 1150 ºC (refer to Figure 4.3), evidence of solid state dissolution of γ' particles was observed. Under these conditions where solid state dissolution has occurred, the morphological and dimensional evolution described above was also observed as a characteristic of dissolution. However, the changes in morphology and size are not unique to solid state dissolution, as this evolution was also evident in samples where liquid state dissolution of some particles had occurred.

### 4.2.2 Liquid State Dissolution

Initially, study of dissolution behaviour of second phase precipitates, such as γ', involved experimentation using conditions of constant heating to a target peak temperature, and long periods of dwell time. As these conditions allow for the material to reach thermodynamic equilibrium during testing, many researchers made the assumption that solid state dissolution was adequate for describing the process of precipitate dissolution. However, in cases where the heating event represents a significant departure from equilibrium, liquid state dissolution may also occur.

The literature review includes an introduction to the 1967 work of Pepe and Savage, who published ground-breaking documentation of constitutional liquation, after observing its

occurrence in the heat-affected zone of welded 18-Ni maraging steel. They observed formation of a liquid film at peak temperatures significantly below the bulk solidus of the material, and explain that the extremely rapid heating rate experienced during welding (greater than 300 ºC/s) can drive non-equilibrium phase transformation. [22] Recall that particle dissolution involves both the dissociation of atoms from the precipitate and the migration of atoms through the matrix. Both reactions must proceed for the particle to dissolve and each mechanism requires sufficient time for the material to maintain thermodynamic equilibrium. [73] At sufficiently rapid heating rates, a very steep concentration gradient is created between the matrix and precipitate, where, in order for both phases to co-exist, a eutectic-like reaction occurs at the particle matrix interface, producing the liquid phase. [22, 74]

Evidence of liquid phase may be observed in the current study in many of the samples where peak temperature has exceeded the practical solvus temperature of γ', 1150 ºC, for Rene 80. The sample shown in Figure 4.11 a) was tested to a peak temperature of T = 1180 ºC, and dwell time of t = 1 second. Many of the γ' particles have liquated and flowed together to form chain-like particle groupings. The hazy film appearance between particles is also characteristic of liquid state dissolution. The yellow arrows highlight liquid film and the black arrows show connected particle groupings. Figure 4.11 b) contains a secondary electron image from a publication of Ola et al [75], also illustrating these characteristics. The sample in Figure 4.11 b) is of substrate Inconel 738 and was heated by Gleeble at a rate of 150 º C/s to 1180 ºC, with a dwell time of 0.5 seconds. In both cases, liquation has been observed to occur at a peak temperature significantly below the solidus temperature of the alloy. Solidus temperatures are reported as 1278 ºC for Rene 80 [12] and 1232 ºC for IN 738. [76]

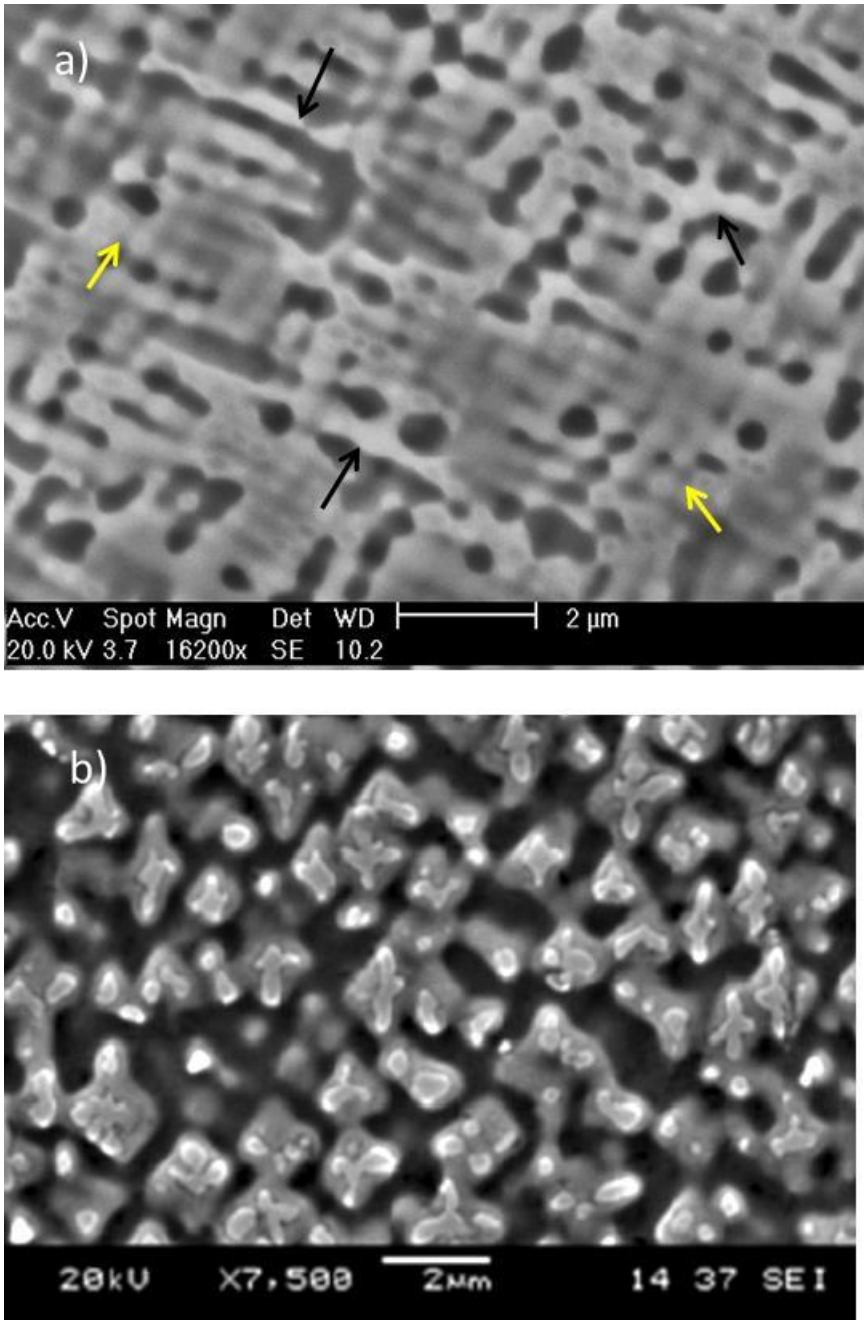


**Figure 4.11: Secondary electron image for a) DS Rene 80 at peak T = 1180 ºC from current study, and b) Inconel 738 sample, reprinted with permission from [75] showing liquation of γ' phase.**

Once a liquid is present, it stands that diffusion would proceed at a faster rate due to higher mobility of atoms in a liquid, and therefore, dissolution of γ' would also proceed quickly to fruition. However, the micrograph in Figure 4.11 a) shows that although there is evidence of liquid state, the γ' phase remains undissolved after 1 second of dwell time at the peak temperature. Particles of γ' phase were also observed in the sample tested to peak T = 1190 ºC. This is an interesting observation for two reasons:

- liquation of the γ' phase has occurred at a temperature below the reported solidus for Rene 80, 1278 ºC [12],
- γ' phase has persisted to temperatures 300 ºC and 400 ºC above the reported solvus for Rene 80.

These observations are not unique to the current work.

Regarding liquation below the equilibrium solidus of a material, after observing constitutional liquation due to rapid heating of Inconel 738, Ojo et al also reviewed micrographs contained in other published works and found additional evidence of constitutional liquation where a rapid heating rate (150ºC/s or faster) was used. [77, 78] Constitutional liquation of gamma prime precipitates has been observed by researchers studying heat-affected zone in nickel-based superalloys after welding. [79] This phenomenon has become an accepted result of rapid heating and is often associated with heating rates experienced during welding processes. Constitutional liquation was also found to be responsible for sub-solidus melting under conditions of controlled low heating rate, though. Sidhu et al. found evidence of incipient melting in Rene 80 occurring at 1160 ºC, after heating as-cast samples using a heating rate of only 2.5 ºC/minute. [80] In this case, the constituents did not consist of coherently existing γ' particles, but of terminal solidification products. For conditions of heating believed to induce equilibrium phase

homogenization, a non-equilibrium liquation reaction occurred. Sidhu et al explain this reaction using the mechanism of constitutional liquation, and indicate that a prior thermodynamic event (cooling from original casting in this case) left the material susceptible to subsequent phase transformation reaction kinetics being altered. [80] The nature of the constituent and history of heating events may therefore be included as contributing factors to the mode of dissolution. Per Ojo's 2004 study, the resultant microstructure following a non-equilibrium heating event is dependent on volume and composition of liquid formed while at peak temperature. [78] Therefore, whether a liquid will form can depend on previous heating events, and on nature of micro-constituents present prior to heating. Also, the degree of liquation and composition of the liquid phase contribute to characteristics of the material subsequent to the non-equilibrium heating event. Due to the occurrence of non-equilibrium environmental conditions producing potentially unexpected microstructural characteristics in different materials, additional research exploring the effects of various parameters is warranted.

Regarding the persistence of second phase particles to remain as precipitates above the established solution temperature, other researchers have also documented this result. Gleeble experiments conducted to simulate welding of IN 738 nickel superalloy involved testing to peak temperatures of up to 1250 ºC using rapid heating rates (>150 ºC/s). [75, 77] These experiments revealed the capability of γ' precipitates to survive as solid particles to temperatures greater than the equilibrium solvus temperature of 1182 ºC [12] for the alloy used. Examination of the microstructure using SEM showed evidence of a liquid film at the interface of some γ' precipitates that managed to persist above temperatures expected to produce complete dissolution. Similarly, a Gleeble simulation study of IN718 by Zhang and Ojo, observed constitutional liquation of delta-phase precipitates. [81] They found δ precipitates ($Ni_3Nb$) able

to persist to temperatures significantly above the equilibrium solidus for the phase and also observed a liquid film below the eutectic temperature. These result are consistent with the observation of γ' precipitates persisting in the current study to a peak temperature of 1190 ºC, and occurrence of liquation below the equilibrium solidus temperature for Rene 80.

### 4.2.3 Stress-assisted Dissolution

Per the previous sections, solid state dissolution is accepted as describing equilibrium-type heating events, as well as may be observed in departures from equilibrium to an extent. Liquid state dissolution is observed in some significant departures from equilibrium in heating events regarded as "transient." However, these two scenarios still do not adequately represent the conditions experienced by blade materials subjected to short-term overtemperature during engine operation. The effects of stress need to be considered as a potential factor in altering the microstructure of material during these unexpected heating events. Because the stress profile of an actual blade is extremely complex and impractical to represent in Gleeble testing, a uniaxial tensile load was used for simplification. Radial stress within an engine is considered to be the maximum net principal stress, and the direction corresponding to this in individual blades is a tensile load from root to tip (i.e. parallel to directionally solidified grains). [1] Uniaxial tensile load has been used in other experimental studies of blade material in order to represent the overall principal stress load of a rotating blade. [39, 46, 49, 50]

For the purposes of showing whether stress can influence dissolution of gamma prime precipitates, a uniaxial tensile load has proven sufficient. Recalling the graphical data presented in Figure 4.9, it is evident that the presence of stress affects particle dissolution. In the cases of both studies, one series of tests completed at peak T = 1050 ºC, one completed at peak T = 1150

ºC, for constant dwell times, and only the tensile load changing, an overall reduction in volume fraction was observed with increasing stress value. This finding offers experimental evidence that tensile stress is a contributing factor in the dissolution process. Following a study simulating the process of linear friction welding, Ola et al asserted that material strain induced by the compressive stresses of LFW produced a higher coefficient of diffusion in the material. [82] In essence, they assert that the relationship $D_{(Strain)} > D_{(No\ Strain)}$ holds true. The greater diffusion coefficient in the presence of strain is credited with inducing rapid phase transformation that may not have proceeded in the absence of the applied stress and therefore strain. An additional study involved both compressive and tensile loading on the same material at peak temperatures representative of welding for short dwell times (0.5 – 10.5s) to observe strain behaviour during LFW. [83] This study produced further evidence of the effects of compressive strain, noting significant constitutional liquation of γ' precipitates in the samples loaded in compression. Samples loaded in tension did not plastically deform prior to failure at any of the test temperatures above T = 1160 ºC. The condition of nil-ductility was determined to be evidence that the relationship between diffusivity in the presence and absence of strain is sign-dependent. Recall equation 2.9 from section 2.2.3, reproduced here for convenience. [33]

$$D_{strain} = D_{unstrained} exp\left(\frac{-Q's}{kT}\right) \qquad \text{(eq. 4.1)}$$

where *Q*' is the activation energy of diffusion per unit strain, and *s* is strain (positive for tensile and negative for compressive). This theory suggests an exponential increase in $D_{strain}$ under compression, but a reduced co-efficient of diffusion in cases of tensile strain. In Ola's experiment, samples that were loaded in tension produced an absence of plastic deformation. These samples were therefore not evaluated for degree of dissolution of γ' precipitates and were

not presented within the article as evidence of the relationship shown in equation 4.1. If the assertions of Cowern et al [33], are revisited, a discrepancy in the argument for sign of strain may be noted. When they presented that equation 4.1 holds true, Cowern et al, also declared the following linear relationship:

$$Q(s) = Q(0) + Q's \qquad \text{(eq. 4.2)}$$

where they define $Q' = dQ/ds$. Because $Q$' is a first order derivative of activation energy as a function of strain, $Q(s)$, it is representative of a change in activation energy with respect to strain ($dQ/ds = \Delta Q$) which may therefore also be negative or positive. This approach allows for an increase in value of $D_{strain}$, even for conditions of tensile strain, and maintains the premise that $D_{(Strain)} > D_{(No\ Strain)}$.

In a study of an austenitic steel alloy containing intermetallic precipitates, tensile samples strained to 6% plastic strain were analyzed using atomic probe tomography. [84] The resulting reduction in quantity and size of intermetallic precipitates was attributed to the applied tensile strain. The authors did not consider diffusion equations in their discussion but instead used dislocation theory to explain the mechanism behind the increase in dissolution. The external application of mechanical load increases the number of dislocations, reducing stability of the precipitates. Reduced stability of a phase means reduced activation energy required for a reaction to proceed which can therefore affect the onset of dissolution. Another study which utilized nuclear magnetic resonance to quantify precipitate dissolution under different known states of strain noted that for that material, a threshold of strain (~30%) was reached, beyond which further assistance to dissolution was not observed. [85] The authors explain that dislocations are capable of shearing the precipitates, which promotes dissociation of solute atoms

from the precipitates and results in solute diffusing back into the matrix. The influence of strain on precipitate dissolution was found to be true only for lower values of strain for that alloy. That strain is a contributing factor but to some threshold value, may explain why there is academic disagreement surrounding the mechanism by which externally applied stress (and therefore strain) affects phase transformation. Some researchers propose that compressive strain only will exponentially increase the diffusion coefficient, thereby increasing dissolution of solute into the matrix. Other researchers assert that any applied mechanical energy will assist in the interface reaction by promoting dissociation of the solute atoms from the precipitate.

Figure 4.9 shows that tensile stress does in fact assist dissolution of gamma prime. Whether the load contributes to the mechanism of atom dissociation or to the migration of atoms requires further study. At a minimum, the results provide a compelling argument that tensile stress should not be disregarded as a contributing factor. Experimental evidence of compressive *and* tensile loading assisting dissolution was documented as a secondary observation in an oxidation study conducted by Foss et al. [86] They exposed a commercial nickel superalloy to 800 ºC in order to study penetration of oxides and found thermo-mechanically tested samples produced an increase in γ' dissolution within the substrate (adjacent to the oxide layer) over samples tested only thermally. An increase in dissolution of γ' was observed both for tensile and compressive loads. However, a greater effect was noted for compression over tension. This supports the observations of current research wherein tensile stress was found to increase dissolution of γ' precipitates.

## 4.3 Kinetics of γ' Dissolution

Analytical models describing the kinetics of precipitate dissolution have been around since the late 1960s, with the prominent contributions made by Whelan in 1969, Aaron, Fainstein & Kotler in 1970, and by Aaron & Kotler in 1971. [28, 30, 31] During the initial research, there was debate about whether precipitate dissolution may be a direct reversal to the process of growth. Eventually, academic agreement was reached that the concentration profile during dissolution was much more complex than for growth, and that the two processes were indeed unique. Despite agreement that dissolution is not simply the reverse process to growth, many analytical models use a "reversed growth" approach to estimate the kinetics. The use of reversed growth may be considered adequate in certain approximations because dissolution, like growth, is often a diffusion-controlled process. One of the greatest difficulties in approximating a diffusion-controlled process is the inherent presence of changing parameters. Recall from Chapter 2, the need for application of an error function in order to solve relatively simple diffusion problems using Fick's 2nd Law. Given the complex nature of the concentration gradient at the interface between a particle and the surrounding matrix, it is not surprising there was disagreement regarding how best to approach a mathematical representation for dissolution. As the study of dissolution behaviour matured, researchers came to agree that for conditions of typical dissolution, describing the kinetics required two components: one to represent a "steady-state" diffusion field and one to represent the co-existing "transient" diffusion field. Per Whelan's 1969 paper [28], dissolution of a spherical precipitate may then be described by the following equation:

$$\frac{dR}{dt} = -\frac{kD}{2R} - \frac{k}{2}\sqrt{\frac{D}{\pi t}} \qquad \text{(eq. 4.3)}$$

where the first term arises from the steady state component of the diffusion field and the second term arises from the transient portion. This implies that the transient diffusion term, in which particle radius (R) is time- (t) dependent, more significantly contributes to the overall rate of change in particle size. It has been found that since over a long time the process will tend toward steady state, conversely, shorter times produce faster rate of dissolution due to the greater effects of the transient component of diffusion. In the present work, the time-dependent study experimentally substantiates that the initial stage of dissolution proceeds very rapidly, the rate slowing as dissolution reaches fruition. To illustrate this point, consider degree of phase transformation to be represented by Y, as per the rate of transformation equation introduced in Chapter 2. If the initial precipitation heat-treated sample represents zero (Y = 0) and complete dissolution of all particles within the matrix represents completion of the phase transformation (Y = 1), then each measure of volume fraction may be assigned values $0 < Y < 1$ representing completion of the dissolution reaction. Figure 4.5 b) shows that in just 20 seconds of dwell time, volume fraction of $\gamma':\gamma$ is reduced from 0.69 to just 0.06, which corresponds to approximately 90% completion of the dissolution reaction. Figure 4.12 illustrates this exponential rate of dissolution.

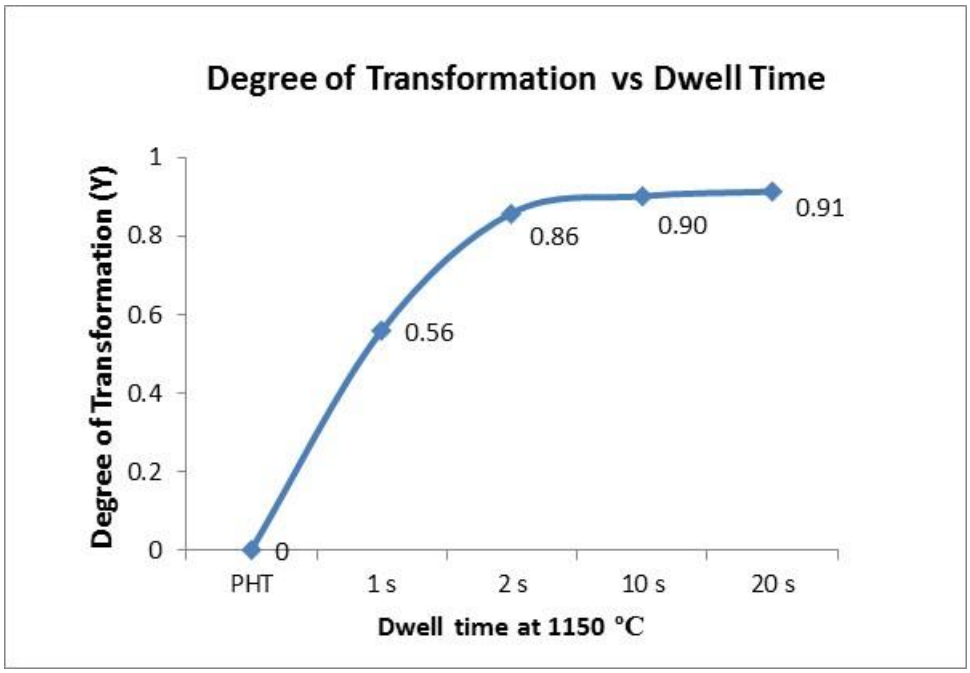


**Figure 4.12: Graphical representation of the dissolution reaction in terms of degree of transformation, Y.**

For phase transformations that produce this shape of curve, rate of transformation may be expressed as follows:

$$\left(\frac{dY}{dt}\right) = [f(Y)]k_0\, exp\left(-\frac{Q}{RT}\right) \qquad \text{(Eq. 4.4) [18]}$$

which may be simplified to $\frac{dY}{dt} = (1-Y)^m k$ , where $k$ represents the exponential value and multiplier $k_0$. For m = 1, and integrating, yields the following:

$$Y = 1 - e^{-kt} \qquad \text{(Eq. 4.5)}$$

Plotting the natural log of (1-Y) versus time then yields a slope of –k and activation energy may be calculated using Equation 4.4. This process requires multiple curves such as the one shown in Figure 4.13, representing the transformation at a series of peak temperatures. This level of

investigation was beyond the scope of the current study, but may be grounds for further research into investigation of activation energy required for $\gamma$' particle dissolution in Rene 80.

The early analytical discussions of dissolution kinetics assume solid state dissolution under "equilibrium" conditions, meaning that "equilibrium" dissolution contains components of both transient and steady state diffusion. For cases of non-equilibrium heating events, the kinetic model is further complicated to include another function representing the dynamically changing environment. In their study of short-term high temperature heating of a single crystal Ni-based superalloy, Cormier et al. investigate dissolution during the dynamically changing environment of a short-term rapid heating event (also referred to as "transient heating regime"). [67] They represent the process of dissolution in terms of $\gamma$':$\gamma$ using a decreasing exponential expression where the actual volume fraction is the sum of volume fraction due to equilibrium conditions and due to the transient conditions. This solution is an attempt at evading the inherent "mathematical" deficiency of dissolved precipitates being dimensionless. When solved using experimental data, their model produced decreasing values of activation energy (Q) and increasing rate constants (k) with increasing temperature, which supports the strong effect of temperature on dissolution kinetics. The model also produced an increase in activation energy values with increased dwell time (isothermal testing), which was explained by the fact that stability of the system increases with increased dwell time, which is also characterized by Figure 4.13 in the current work. Finally, they calculated an overall "apparent activation energy," Q = 190 kJ/mol, which they assert is characteristic of $\gamma$' dissolution during transient heating regimes. [67] Compared to the reported activation energies for diffusion of Al through Ni (249 kJ/mol), and self-diffusion of Ni (285 kJ/mol) [87], this value is significantly lower. Using the value of Q as an indicator whether or not dissolution will initiate, Cormier et al. [67], concluded their study

by offering that the lower calculated activation energy is indicative of the effect of departure from equilibrium on phase stability. Experimental observations in the current work support the premise that short-term non-equilibrium heating events decrease phase stability and are capable of initiating non-equilibrium dissolution.

An investigation into the effects of strain on the dissolution kinetics of γ' precipitates in a single crystal Ni-base superalloy provided experimental evidence that an applied load enhanced the rate of dissolution. The study involved equilibrium as well as transient heating regimes in both loaded and unloaded conditions. In agreement with the thermal testing presented in Figure 4.5, Giraud et al. [66] found the greatest decrease in volume fraction to occur in the shortest dwell times (where $t < 1$ minute) and found that transient heating regime produced dissolution at temperatures significantly below the γ' solvus for the alloy. When load was introduced, they observed an increase in dissolution kinetics with increased plastic strain. Further assessment of the data led them to theorize that strain accelerates γ' dissolution (in CMSX-4) to a threshold of 0.3% strain, and beyond that threshold, kinetics are only thermally driven. The increase in dissolution kinetics due to applied stress was attributed to the increase in density of dislocations at the γ':γ interface. [66] The potential of a strain threshold beyond which mechanical load ceases to contribute to the kinetics of dissolution is also an interesting finding. Although existing plastic strain as well as applied load were believed to assist dissolution kinetics, the authors were careful to explain that no systematic comparison of dissolution of γ' particles with and without applied stress has been performed. A study by Cormier et al, published in 2008 [88], does directly compare dissolution kinetics of γ' particles in the presence and absence of applied stress. They found that applied stress accelerated the dissolution process and that larger stress produced a greater reduction in volume fraction of γ' for the same dwell time. Regarding

the current investigation, the applied tensile stress also produced a greater reduction in volume fraction. Once dissolution has begun, whether thermally activated or stress assisted, the rate of dissolution has been found to proceed more quickly during initial stage of the reaction.

Finally, because both solid state and liquid state dissolution have been observed, comments must also be made regarding the effects of constitutional liquation on dissolution kinetics. It has already been stated that the solid state (isothermal) dissolution kinetic model includes components of transient and steady state diffusion. Adding a dynamically changing temperature during rapid short-term heating events adds complexity to that model. It was suggested that stress can contribute to kinetics of reactions occurring at the interface. When the interface reaction also includes the potential for formation of a liquid film, even further complexity to the dissolution kinetics is introduced. Other authors have researched liquid film migration and its kinetics, but the application as it may relate specifically to altering the dissolution kinetics of γ' precipitates is beyond the scope of this project. Analytical solutions for a system that models precipitate dissolution in a transient heating regime and addresses constitutional liquation were not discovered by this author. However, it is known that as a non-equilibrium mode of dissolution, constitutional liquation has the potential to alter the kinetics of subsequent heating events producing unexpected reactions such as sub-solidus incipient melting. [80]

# Chapter 5

## Summary and Conclusions

Nickel superalloys, ideal for use in gas path or hot section environments within gas turbine aero- and power generation engines, are composed of a high volume fraction of strength-inducing gamma-prime (γ') precipitate phase within a gamma (γ) matrix. During normal engine operation, rotating gas path components such as first stage turbine blades experience temperatures greater than 1000 ºC while under load and in the presence of corrosive gases, and the superalloys are designed to retain strength and perform well in this environment. An operational condition known as short-term overtemperature may cause components such as turbine blades to experience brief spikes in temperature where there may be risk of the strengthening γ'-phase dissolving, thereby potentially reducing strength of the material. The actual microstructural effects of transient heating regimes such as short-term overtemperature are not well-documented and have been investigated for a specific set of parameters in the current work. Experiments simulating short-term overtemperature by heating at a constant rapid heating rate, representative of typical engine start to varying peak temperatures within a range known to induce precipitate dissolution, for varying dwell times and under increasing applied tensile loads, were conducted using Gleeble thermo-mechanical simulation.

## 5.1 Summary of Findings

For the studies involving thermal- and thermo-mechanical simulations to varying peak temperatures, dwell times, and conditions of tensile load, the following observations were made:

1. Volume fraction of γ': γ was found to reduce with increasing peak temperature for a constant heating rate and constant dwell time. Dissolution was found to occur over a range of temperatures where some evidence of dissolution was observed at 1130 ºC and only a very small percentage of particles remained undissolved at 1190 ºC.

2. Volume fraction of γ': γ was found to decrease with increasing dwell time at the peak test temperature coinciding with the practical solvus temperature of γ'. A significant percentage of γ' phase (over 90% from original volume fraction) had completely dissolved in just 20 seconds dwell time. These data reflect the general acceptance that reaction kinetics are significantly faster at the onset of dissolution and slow as steady state is reached and the ratio of precipitate to matrix approaches zero.

3. Precipitates dissolved primarily by solid state dissolution up to temperatures of 1150 ºC, but evidence of constitutional liquation (liquid state dissolution) was observed in samples heated to peak temperature of 1150 ºC and greater. Some γ' precipitates were found to persist to temperature of 1190 ºC, due to the phenomenon of constitutional liquation limiting atomic mechanism required for complete dissolution to proceed.

4. An applied tensile stress was found to influence precipitate dissolution such that volume fraction was reduced with the application of load compared to unloaded samples when other parameters were held constant. The effect of stress was more pronounced for samples exposed to the higher peak temperature of 1150 ºC than for 1050 ºC.

## 5.2 Suggestions for Future Research

- Heating rate was constant for all testing within current research, and was selected based on engine start as a typical event to induce short-term overtemperature. Review of other research shows that heating rate can significantly affect the range of temperature over which precipitate dissolution occurs, and also cause a shift in the "practical" dissolution temperature of the γ' precipitate phase. Additional studies utilizing slower heating rates or involving smaller temperature differentials potentially more representative of in-flight temperature spikes may produce different results.

- Unrecoverable hardware failure in the Gleeble apparatus led to modification of experimentation (limited ability to conduct testing on timed and loaded samples). Strain was not measured during experimentation; only stress was considered. Given that other researchers propose that diffusivity is dependent on both sign and magnitude of an applied strain, it stands that further testing to investigate the effects of both compressive and tensile strain is warranted.

- Many precipitate strengthened Ni-based superalloys contain a bi-modal structure of gamma prime (beginning with 2-stage aging to produce coarse primary and fine secondary) when in optimal heat-treated condition. The bi-modal microstructure is a factor to be considered as possessing a potentially different response to short-term overtemperature events given that original precipitate size (and morphology) as well as volume fraction may both contribute to activation energy required for dissolution to initiate.

- Only the on-heating process was analyzed in the current study, with simulated samples quenched at peak temperature. This allowed for information to be gained on the response of microstructure to the heating event. However, understanding of the material's potential ability to be restored to a favourable condition of γ'-γ volume fraction through re-precipitation of γ' at regular service temperatures remains an unstudied phenomenon.

Given the importance of the relationship between the strengthening phase of gamma prime precipitates and the gamma matrix in nickel-based superalloys, it is not surprising that researchers have worked to study variations of environmental changes the material could potentially experience in many industrial applications. The current work illustrates evidence of the dynamic effects time, temperature and uniaxial stress on microstructure of the directionally solidified nickel based superalloy Rene 80, discusses the complex nature in which these parameters are inter-related and indicates how additional research on this topic could potentially benefit industry.

# 6.0 –References


[1] C. T. Sims, N. Stoloff and W. C. Hagel, Superalloys II, New York: Joh Wiley & Sons, 1987.

[2] C. T. Sims, "A History of Superalloy Metallurgy for Superalloy Metallurgists," General Electric Company, Schenectady, 1984.

[3] W. L. Mankins and S. Lamb, "Nickel and Nickel Alloys," in *Volume 2, Properties and Selection: Nonferrous Alloys and Special Purpose Materials*, ASM International, 1992, pp. 428-445.

[4] M. J. Donachie and S. J. Donachie, "Superalloys: A Technical Guide," in *ASM Handbook: Nonferrous Alloys*, 2nd ed., ASM International, 2002, pp. 1-24.

[5] J. Johnson and M. J. J. Donachie, "Microstructure of Precipitation Strengthened Nickel-Base Superalloys," in *National Metal Congress*, Chicago, 1966.

[6] D. Muzyka, "Controlling Microstructures and Properties of Superalloys Via Use of Precipitated Phases," *Metals Engineering Quarterly,* no. November, pp. 12-20, 1971.

[7] M. Gell, D. N. Duhl and A. F. Giamei, "The Development of Single Crystal Superalloy Turbine Blades," Pratt & Whitney Aircraft Group, Hartford, 1980.

[8] C. P. Sullivan and M. J. J. Donachie, "Some Effects of Microstructure on the Mechanical

Properties of Nickel-Base Superalloys," *Metals Engineering Quarterly,* pp. 250-259, February 1967.

[9] Y. Nakagawa, A. Ohtomo and Y. Saiga, "Directional Solidification of Rene 80," *Transactions of the Japan Institue of Metals,* vol. 17, no. 6, pp. 323-329, 1976.

[10] ASM International, "Compositions of Superalloys," 2011. [Online]. Available: Http://products.asminternational.org. [Accessed 21 May 2013].

[11] J. Lecomte-Beckers, "Study of Solidification Features of Nickel-base Superalloys in Relation with Composition," *Metallurgical Transactions A,* vol. 19A, no. 9, pp. 2333-2340, 1988.

[12] D. L. Sponseller, "Differential Thermal Analysis of Nickel-Base Superalloys," *Superalloys,* pp. 259-270, 1996.

[13] L. Zimina, N. Burova and O. Makushok, "Effect of Hafnium on the Structure and Properties of Wrought Nickel-base Alloys," *Metal Science and Heat Treatment,* vol. 28, no. 2, pp. 130-135, 1986.

[14] J. Safari and S. Nategh, "On the Heat Treatment of Rene-80 Nickel-base Superalloy," *Journal of Materials Processing Technology,* no. 176, pp. 240-250, 2006.

[15] General Electric, "Nonferrous Alloys, Code 4214," in *Aerospace Structural Metals Handbook*, ASM, 1982, pp. 1-18.

[16] T. M. Pollock and S. Tin, "Nickel-Based Superalloys for Advanced Turbine Engines: Chemistry, Microstructure, and Properties," *Journal of Propulsion and Power,* vol. 22, no. 2, pp. 361-374, 2006.

[17] G. Maniar, J. Bridge Jr., H. James and G. Heydt, "Correlation of Gamma-Gammma Prime Mismatch and Strengthening in Ni/Fe-Ni Base Alloys Containing Alumiinum and Titanium as Hardeners," *Metallurgical Transactions,* vol. 1, pp. 31-42, January 1970.

[18] A. K. Jena and M. C. Chaturvedi, Phase Transformations in Materials, Prentice Hall, 1991.

[19] Key to Metals AG, "Nickel-Based Superalloys: Part One," January 2010. [Online]. Available: http://www.keytometals.com/superalloys. [Accessed 29 March 2013].

[20] H. J. Kolkman, "Coarsening and Solutioning of Precipitates in Superalloys," National Aerospace Labratory, Amsterdam, 1983.

[21] M. Soucail and Y. Bienvenu, "Dissolution of the Gamma' Phase in a Nickel Base Superalloy at Equilibrium and Under Rapid Heating," *Materials Science and Engineering,* vol. A, no. 220, pp. 215-222, 1996.

[22] J. Pepe and W. Savage, "Effects of Constitutional Liquation in 18-Ni Maraging Steel Weldments (Microsegregation and grain boundary liquation in heat affected zone of 18-Ni maraging steel welds)," *Welding Journal,* vol. September Welding Research Supplement, no.

46, pp. 412-s - 422-s, 1967.

[23] O. Ojo, On Liquation Cracking of Cast Inconel 738LC Superalloy Welds, Winnipeg: University of Manitoba, 2004.

[24] O. T. Ola, "Microstructural Analysis of Linear Friction Welded Joint in Nickel-base Inconel 738 Superalloy," University of Manitoba, Winnipeg, 2010.

[25] W. D. J. Callister, Materials Science and Engineering: An Introduction, 2nd ed., New York: John Wiley & Sons Inc., 1991.

[26] H. Mehrer, Diffusion in Solids: Fundamentals, Methods, Materials, Diffusion-controlled Processes, Chicago: Springer, 2007.

[27] H. Aaronson, M. Enomoto and J. Lee, Mechanisms of Diffusional Phase Transformations in Metals and Alloys, Taylor & Francis Group, 2010.

[28] M. J. Whelan, "On the Kinetics of Precipitate Dissolution," *Metal Science Journal,* vol. 3, pp. 95-97, 1969.

[29] V. Raghavan, Materials Science and Engineering: A First Course, New Delhi: PHI Learning Private Limited, 2010.

[30] H. Aaron, D. Fainstein and G. Kotler, "Diffusion-Limited Phase Transformations: A Comparison

and Critical Evaluation of the Mathematical Approximations," *Journal of Applied Physics,* vol. 41, no. 11, pp. 4404-4410, 1970.

[31] H. Aaron and G. Kotler, "Second Phase Dissolution," *Metallurgical Transactions,* vol. 2, pp. 393-408, 1971.

[32] A. Ardell and V. Ozolins, "Trans-Interface Diffusion-controlled Coarsening," *Nature Materials,* vol. 4, pp. 309-316, 2005.

[33] N. Cowern, P. Zalm, P. van der Sluis, D. Gravesteijn and W. de Boer, "Diffusion in Strained Si(Ge)," *Physical Review Letters,* vol. 72, no. 16, pp. 2585-2588, 1994.

[34] A. Antonelli and J. Bernholc, "Pressure Effects on Self-diffusion in Silicone," *Physical Review B,* vol. 40, no. 15, pp. 10643-10646, 1989.

[35] N. Cowern, "Diffusion in a Single Crystal within a Stressed Environment," *Pysical Review Letters,* vol. 99, no. 155903, pp. 1-4, 2007.

[36] A. Antonelli and J. Bernholc, "Pressure and Strain Effects on Diffusion," in *Materials Research Society Online Proceedings Library*, 1989.

[37] GE Power Systems, *Gas Turbine Repair Technology,* GE Power Systems, 2001.

[38] A. Baldan, "Review: Progress in Ostwald Ripening Theories and Their Applications to Ni-base

Alloys," *Journal of Materials Science,* no. 37, pp. 2171-2202, 2002.

[39] S. L. Draper, D. R. Hull and R. L. Dreshfield, "Observations of Directional Gamma Prime Coarsening During Engine Operation," NASA, Denver, 1987.

[40] Ardell, "The Growth of Gamma Prime Precipitates in Aged Ni-Ti Alloys," *Metallurgical Transactions,* vol. 1, pp. 525-534, February 1970.

[41] D. Hadjiapostolidou and B. Shollock, "Long Term Coarsening in Rene 80 Ni-Base Superalloy," in *Superalloys*, London, The Minerals, Metals & Materials Society, 2008, pp. 733-739.

[42] J. Safari, S. Nategh and M. McLean, "Evolution of Microstructure of Nickel Base Superalloy at High Temperatures," *Materials Science and Technology,* vol. 22, no. 8, pp. 888-898, 2006.

[43] R. Stevens and P. Flewitt, "The Effects of Gamma' Precipitate Coarsening during Isothermal Agind and Creep of the Nickel-base Superalloy IN-738," *Materials Science and Engineering,* vol. 37, pp. 237-247, 1979.

[44] E. Balikci and A. Raman, "The Relationship Between Activation Energy and Precipitate Size for Precipitate Agglomeration," *Materials Science,* vol. 43, pp. 927-932, 2008.

[45] T. Ichitsubo, D. Koumoto, M. Hirao, K. Tanaka, M. Osawa, T. Yokokawa and H. Harada, "Rafting Mechanism for Ni-base SuperalloyUnder External Stress: Elastic or Elastic-Plastic Phenomena?," *Acta Materialia,* vol. 51, pp. 4033-4044, 2003.

[46] M. Kamaraj, "Rafting in Single Crystal Nickel-base Superalloys--An Overview," *Sadhana,* vol. 28, no. 2, pp. 115-128, 2003.

[47] F. R. N. Nabarro, "Rafting in Superalloys," *Metallurgical and Materials Transactions,* vol. 27A, pp. 513-530, 1996.

[48] J. Lapin, T. Pelachova and M. Gebura, "Microstructure degradation of Nickel Based Single Crystal Superalloy During Creep," in *Metal 2012*, Brno, Czech Republic, 2012.

[49] S. Li, J. Tao, T. Sugui and H. Zhuangqi, "Influence of Precipitate Morphology on Tensile Creep of a Single Crystal Nickel-base Superalloy," *Materials Science and Engineering,* vol. A, no. 454-455, pp. 461-466, 2007.

[50] R. A. MacKay and L. J. Ebert, "The Development of Gamma-Gamma Prime Lamellar Structures in a Nickel-Base Superalloy during Elevated Temperature Mechanical Testing," *Metallurgical Transactions,* vol. 43, no. 16A, pp. 1969-1985, 1985.

[51] Transport Canada, *Canadian Aviation Regulation 533: Aircraft Engines,* Government of Canada, 2015.

[52] B. R. Junkin, Interviewee, *Assessment of Blades Subjected to Customer-reported Short-term Overtemperature.* [Interview]. 10 June 2013.

[53] J. Hou, B. Wicks and R. Antoniou, "An Investigation of Fatigue Failures of Turbine Blades in a Gas Turbine Engine by Mechanical Analysis," *Engineering Failure Analysis,* vol. 9, no. 2, pp. 201-211, 2002.

[54] Z. Mazur, A. Luna-Ramirez, J. Juarez-Islas and A. Campos-Amezcua, "Failure analysis of a gas turbine blade made of Inconel 738LC alloy," *Engineering Failure Analysis,* vol. 12, pp. 474-486, 2005.

[55] R. Rajendran, M. Caneshachar, T. Jivankumar and R. Mohana, "Condition Assessment of Gas Turbine Blades and Coatings," *Engineering Failure Analysis,* vol. 18, pp. 2104-2110, 2011.

[56] R. Knoerr, "In Flight Shutdowns Resulting from HPT Blade Distress due to Harsh Environment," Transport Canada, 2016.

[57] B. Goyaniuk, " Compressor Turbine Blades," Government of Canada, 2007.

[58] Pratt & Whitney Canada, *Proprietary Information,* Montreal: PWC, 2010.

[59] ASTM, *Rectangular Tension Test Specimen,* American Standards and Testing, 2004.

[60] D. Brexton, *Standard Practice for Determining Volume Fraction by Systematic Manual Point Count,* American Standards and Testing, 1990.

[61] C. Yang, Y. Xu, H. Nie, X. Xiao, G. Jia and Z. Shen, "Effects of Heat Treatments on the

Microstructure and Mechanical Properties of Rene 80," *Materials and Design,* no. 43, pp. 66-73, 2013.

[62] C. W. Andrews, "Volume Fraction Determination in Cast Superalloys and DS Eutectic Alloys by a New Practice for Manual Point Counting," NASA, Cleveland, 1976.

[63] M. Cieslak, T. Headley, T. Kollie and A. Romig, "A Melting and Solidification Study of Alloy 625," *Metallurgical Transactions A,* vol. 19A, no. September, pp. 2319-2331, 1988.

[64] H. Saari, D. Seo, J. Blumm and J. Beddoes, "Thermophysical Property Determination of High Temperature Alloys by Thermal Analysis," *Journal of Thermal Analysis and Calorimetry,* vol. 73, pp. 381-388, 2003.

[65] Zla, Smetana, Zaludova, Dobrovska, Vodarek, Konecna, Matejka and Francova, "Determination of Thermophysical Properties of High Temperature Alloy IN713LC by Thermal Analysis," *Journal of Thermal Alaysis & Calorimetry,* vol. 110, no. 1, pp. 211-219, 2012.

[66] R. Giraud, Z. Hervier, J. Cormier, G. Saint-Martin, F. Hamon, X. Milhet and J. Mendez, "Strain Effect on the γ’ Dissolution at High Temperatures of a Nickel-Based Single Crystal Superalloy," *Metallurgical and Materials Transactions A,* vol. 44A, no. January, pp. 131-146, 2013.

[67] J. Cormier, X. Milhet and J. Mendez, "Effect of Very High Temperature Short Exposures on the Dissolution of the Gamma' Phase in Single Crystal MC2 Superalloy," *Journal of Material*

*Science,* vol. 42, no. June, pp. 7780-7786, 2007.

[68] E. Balikci and A. Raman, "Characteristics of the Gamma Prime Precipitates at High Temperatures in Ni-base Polycrystalline Superalloy IN738LC," *Journal of Materials Science,* vol. 35, pp. 3593-3597, 2000.

[69] A. Thakur, "Microstructural Responses of a Ni-based Cast IN-738 Superalloy to a Variety of Pre-Weld Heat Treatment," University of Manitoba, Winnipeg, 1997.

[70] T. Wang, X. Wang, Z. Zhao and Z. Zhang, "Dissolution Behaviour of the Gamma' Precipitates in Two Kinds of Ni-based Superalloys," *Materials at High Temperatures,* vol. 33, no. 1, pp. 51-57, 2016.

[71] A. Maheshwari and A. Ardell, "Morphological Evolution of Coherent Misfitting Precipitates in Anisotropic Elastic Media," *Physical Review Letters,* vol. 70, no. 15, pp. 2305-2308, 1993.

[72] S. Onaka, N. Koriko, T. Fujii and M. Kato, "Simplified Energy Analysis on the Equilibrium Shape of Coherent γ’ Precipitates in γ Matrix with a Superspherical Shape Approximation," *Intermetallics,* vol. 10, pp. 343-346, 2002.

[73] J. Martin and R. Doherty, Stability of Microstructure in Metallic Systems, Cambridge: Cambridge University Press, 1976.

[74] J. Pepe and W. F. Savage, "Weld Heat-Affected Zone of the 18-Ni Maraging Steels," *Welding*

*Journal,* vol. Welding Research Supplement, no. December, pp. 545-s - 553-s, 1970.

[75] O. Ola, O. Ojo, P. Wanjara and M. Chaturvedi, "Analysis of Microstructural Changes Induced by Linear Friction Welding in a Nickel-based Superalloy," *Metallurgical and Materials Transactions A,* vol. 42, no. 12, pp. 3761-3777, 2011.

[76] International Nickel Company, Inc. (INCO), "Alloy IN-738 Technical Data," New York.

[77] O. Ojo and M. Chaturvedi, "On the Role of Liquated Gamma Prime Precipitates in Weld Heat Affected Zone Microfissuring of a Nickel Based Superalloy," *Materials Science and Engineering A,* no. 403, pp. 77-86, 2005.

[78] O. Ojo, N. Richards and M. Chaturvedi, "Contribution of Constitutional Liquation of Gamma Prime Precipitate to Weld HAZ Cracking of Cast Inconel 738 Superalloy," *Scripta Materialia 50,* pp. 641-646, 2004.

[79] L. Lim, J. Yi, N. Liu and Q. Ma, "Mechanism of Post-Weld Heat Treatment Cracking in Rene 80, Nickel Based Superalloy," *Materials Science and Technology,* vol. 18, no. April, pp. 407-412, 2002.

[80] R. Sidhu, O. Ojo and M. Chaturvedi, "Sub-solidus Melting of Directionally Solidified Rene 80 Superalloy During Solution Heat Treatment," *Journal of Materials Science,* no. 43, pp. 3612-3617, 2008.

[81] H. Zhang and O. Ojo, "Non-equilibrium Liquid Phase Dissolution of δ Phase Precipitates in a Nickel-based Superalloy," *Philisophical Magazine Letters,* vol. 89, no. 12, pp. 787-794, 2009.

[82] O. Ola, O. Ojo, T. Wanjara and M. Chaturvedi, "Enhanced Resistance to Weld Cracking by Strain-induced Rapid Solidification during Linear Friction Welding," *Philisophical Magazine Letters,* vol. 91, no. 2, pp. 140-149, 2011.

[83] O. Ola, O. Ojo and M. Chaturvedi, "Effect of Deformation Mode on Hot Ductility of a Gamma' Preciipitation Strengthened Nickel-base Superalloy," *Materials Science & Engineering A,* vol. 585, pp. 319-325, 2013.

[84] Z. Jiao, M. McMurtrey and G. Was, "Strain-induced Precipitate Dissolution in an Irradiated Austenitic Allloy," *Scripta Materialia,* vol. 65, no. 2, pp. 159-162, 2011.

[85] C. Hutchinson, P. Loo, T. Bastow, A. Hill and J. da Costa Teixeira, "Quantifying the Strain-induced Dissolution of Precipitates in Al Alloy Microstructures Using Nuclear Magnetic Resonance," *Acta Materialia,* vol. 57, no. 19, pp. 5645-5653, 2009.

[86] B. Foss, M. Hardy, D. Child, D. McPhail and B. Shollock, "Oxidation of a Commercial Nickel-base Superalloy under Static Loading," *Journal of the Minerals, Metals and Materials Society,* vol. 66, no. 12, pp. 2516-2524, 2014.

[87] R. Weast, Handbook of Chemistry and Physics, 66th ed., CRC Press, 1985.

[88] J. Cormier, X. Milhet, J.-L. Champion and J. Mendez, "Simulation of Very High Temperature Overheating During Isothermal Creep of Single Crysta lNi-Base Superalloy," *Advanced Engineering Materials,* vol. 10, no. 1-2, pp. 56-61, 2008.